Mitochondrial biogenesis is transcriptionally repressed in lysosomal lipid storage diseases

King Faisal Yambire[1,2,3], Lorena Fernández Mosquera[1], Robert Steinfeld[4], Christiane Muhle[5], Elina Ikonen[6], Ira Milosevic[3], Nuno Raimundo[1,#]

[1]Institute of Cellular Biochemistry, University Medical Center Goettingen, Germany

[2]International Max-Planck Research School in Neuroscience, Goettingen, Germany

[3]European Neuroscience Institute, Goettingen, Germany

[4]Klinik für Kinder- und Jugendmedizin, University Medical Center Goettingen, Germany

[5]Department of Psychiatry and Psychotherapy, Friedrich-Alexander University Erlangen-Nürnberg (FAU), Erlangen, Germany

[6]Biomedicum Helsinki, University of Helsinki, Faculty of Medicine, Department of Anatomy, Helsinki, Finland

[#]corresponding author: Nuno Raimundo

Email: nuno.raimundo@med.uni-goettingen.de

Telephone: +49 551 3912809

Fax: +49 551 395979

ABSTRACT

Perturbations in mitochondrial function and homeostasis are pervasive in lysosomal storage diseases, but the underlying mechanisms remain unknown. Here, we report a transcriptional program that represses mitochondrial biogenesis and function in lysosomal storage diseases Niemann-Pick type C (NPC) and acid sphingomyelinase deficiency (ASM), in patient cells and mouse tissues. This mechanism is mediated by the transcription factors KLF2 and ETV1, which are both induced in NPC and ASM patient cells. Mitochondrial biogenesis and function defects in these cells are rescued by the silencing of KLF2 or ETV1. Increased ETV1 expression is regulated by KLF2, while the increase of KLF2 protein levels in NPC and ASM stems from impaired signaling downstream sphingosine-1-phosphate receptor 1 (S1PR1), which normally represses KLF2. In patient cells, S1PR1 is undetectable at the plasma membrane and thus unable to repress KLF2. This manuscript provides a mechanistic pathway for the prevalent mitochondrial defects in lysosomal storage diseases.

INTRODUCTION

Lysosomal storage diseases are a group of severe diseases caused by mutations in genes encoding for lysosomal proteins, and are referred to as storage diseases because one common phenotype is the accumulation of undigested substrates in the lysosomes, with the consequent enlargement and loss of function of the organelle (Parenti et al., 2015). The lysosomes have far-reaching roles beyond the “recycling bin” paradigm, and are key players in nutrient sensing and metabolic regulation (Ballabio, 2016; Lim and Zoncu, 2016; Settembre et al., 2013). Furthermore, lysosomes are essential for the process of macroautophagy, and thus for the selective autophagy of mitochondria, the main mechanism to degrade dysfunctional mitochondria (Pickles et al., 2018). Mitochondrial perturbations have been widely reported in several lysosomal storage diseases (Platt et al., 2012; Plotegher and Duchen, 2017), including neuronal ceroid lipofuscinosis, Gaucher and Niemann-Pick diseases (Jolly et al., 2002; Lim et al., 2015; Osellame et al., 2013; Torres et al., 2017; Wos et al., 2016). Nevertheless, it remains unclear why mitochondrial dysfunction is so prevalent in lysosomal storage diseases.

In this study, we focus on two lysosomal storage diseases, Niemann-Pick type C (NPC) and acid sphingomyelinase deficiency. NPC is caused by mutations in the gene *NPC1* or, less commonly, *NPC2* (Patterson and Walkley, 2017; Schuchman and Wasserstein, 2016). *NPC1* and *NPC2* encode proteins involved in sphingomyelin and cholesterol efflux from the lysosome (Platt, 2014). Acid sphingomyelinase deficiency, also known as Niemann-Pick A/B, is caused by mutations in the gene *SMPD1* encoding acid sphingomyelinase (ASM). ASM catalyzes the breakdown of sphingomyelin into ceramide and phosphorylcholine (Schuchman and Wasserstein, 2016). Interestingly, accumulation of cholesterol, sphingosine, sphingomyelin and glycosphingolipids in the lysosomes are observed both in Niemann-Pick and acid sphingomyelinase deficiency cells and tissues (Leventhal et al., 2001; Vanier, 1983).

The NPC1 knock-out mouse ($NPC1^{-/-}$) and a knock-in of the most common NPC1 patient mutation I1061T (Praggastis et al., 2015) are established models of Niemann-Pick type C disease (Loftus et al., 1997). Both $NPC1^{-/-}$ and $NPC1^{I1061T}$ mice recapitulate most of the neuropathological phenotypes of the disease, with the disease onset occurring earlier in the $NPC1^{-/-}$ mice. The ASM knock-out mouse ($ASM^{-/-}$) is a widely used model of ASM deficiency (Horinouchi et al., 1995).

Mitochondria are fundamental metabolic organelles in the cell, harboring key pathways for aerobic metabolism such as the citrate cycle, the key integrator metabolic pathway, as well as the respiratory chain and oxidative phosphorylation, Fe-S cluster and heme synthesis (Pagliarini and Rutter, 2013). They are also recognized as a major cellular signaling platform, with far-reaching implications on cell proliferation, stem cell maintenance, cellular immunity and cell death (Kasahara and Scorrano, 2014; Raimundo, 2014). Mitochondria are composed of about 1000 proteins, of which only 13 are encoded by mitochondrial DNA (mtDNA) (Pagliarini et al., 2008). The other ˜1000 proteins are encoded by nuclear genes, and imported to the different sub-mitochondrial compartments (e.g., matrix, inner membrane, outer membrane, intermembrane space) by dedicated pathways (Wiedemann and Pfanner, 2017).

The large number of proteins that are nuclear-encoded and imported to mitochondria imply the need for regulatory steps that ensure the coordination of the process of mitochondrial biogenesis. This is often regulated at transcript level, by transcription factors that promote the expression of nuclear genes encoding for mitochondrial proteins (Scarpulla et al., 2012). One of the best characterized is the nuclear respiratory factor 1 (NRF1), which stimulates the expression of many subunits of the respiratory chain and oxidative phosphorylation, but also of genes necessary for mtDNA maintenance and expression, such as TFAM (Evans and Scarpulla, 1989, 1990). Other transcription factors, such as estrogen-related receptor α (ERRα) and the oncogene myc, also act as positive regulators of mitochondrial biogenesis (Herzog et al., 2006; Li et al., 2005). Several co-activators also participate in the regulation of

mitochondrial biogenesis, of which the co-activator PGC1α (peroxisome proliferator-activated receptor-gamma, co-activator 1 α) is the best characterized (Wu et al., 1999). PGC1a can interact with NRF1 or ERRα and stimulate mitochondrial biogenesis (Scarpulla et al., 2012). No transcriptional repressors of mitochondrial biogenesis have so far been described. Impaired or uncoordinated mitochondrial biogenesis often results in impaired mitochondria leading to pathological consequences (Cotney et al., 2009; Raimundo et al., 2012).

Here, we identify the transcription factors KLF2 and ETV1 as transcriptional repressors of mitochondrial biogenesis. The up-regulation of these two proteins in patient cells and mouse tissues of two lysosomal diseases, Niemann-Pick type C and ASM deficiency, underlies the mitochondrial defects observed in these syndromes. The silencing of ETV1 and, particularly, KLF2, is sufficient to return mitochondrial biogenesis and function to control levels.

RESULTS

Expression of mitochondria-related genes is decreased in NPC1$^{-/-}$ tissues

Mitochondrial homeostasis and function is impaired in many lysosomal storage diseases. The two main axes of mitochondrial homeostasis are biogenesis and demise (by selective autophagy, designated mitophagy). Given that lysosomal diseases are characterized by impaired autophagy (Settembre et al., 2008), it is expectable that mitophagy is also impaired. However, it remains unknown how mitochondrial biogenesis is affected in lysosomal storage diseases.

To assess mitochondrial biogenesis at transcript level in a systematic manner, we resorted to a publicly-available transcriptome dataset of NPC1$^{-/-}$ mice liver and brain, the two tissues most affected in Niemann-Pick type C. The dataset included both pre-symptomatic and symptomatic animals (Alam et al., 2012). To monitor the effects of Niemann-Pick disease on transcriptional regulation of mitochondrial biogenesis, we started by establishing a comprehensive list of mitochondria-related genes. We used a published mitochondrial proteome (MitoCarta, (Pagliarini et al., 2008) see methods for details), and converted the protein names to the corresponding ENSEMBL gene name to generate the “mitochondria-associated gene list”. The process is illustrated in Figure 1A. We prepared a second list which included only the respiratory chain and oxidative phosphorylation subunits (“RC/OXPHOS gene list”). As controls, we prepared “gene lists” for lysosomes, peroxisomes, Golgi and endoplasmic reticulum using the same strategy. The proteomes used to build the organelle-specific gene lists are detailed in the methods section (Table I). Next, we used transcriptome data from asymptomatic and symptomatic brain and liver of NPC1$^{-/-}$ and corresponding WT littermates to determine how the organelle gene lists were affected.

First, we assessed the average expression of lysosomal genes in NPC1$^{-/-}$ brain and liver, to verify the validity of our “organelle gene list” approach in this dataset. We have shown earlier that the average expression level of an organelle-gene list is a good indicator of the activity of the transcriptional program of biogenesis for that organelle (Fernandez-Mosquera et al.,

2017). The average expression of lysosomal genes was significantly increased in the asymptomatic NPC1$^{-/-}$ brain and liver (Supplementary Figure S1A), and increased further with the onset of the disease in NPC1$^{-/-}$ brain and liver (Supplementary Figure S1A), in agreement with the expected increase in the expression of lysosomal genes in lysosomal storage diseases.

Then, we measured the average expression of the "mitochondrial gene list" in NPC1$^{-/-}$ brain and liver. Mitochondria-associated genes were up-regulated in pre-symptomatic NPC1$^{-/-}$ brain, and down-regulated in symptomatic brain (Figure 1B). In the liver, the average expression of mitochondria-associated genes was not significantly changed in the pre-symptomatic group, but was robustly decreased in the symptomatic NPC1$^{-/-}$ mice (Figure 1B). When looking only at the "RC/OXPHOS gene list", the pattern was similar but the magnitude of the changes was more robust (Figure 1C). These results are not due to a small number of genes skewing the whole population, since the proportion of mitochondrial genes in the differentially expressed gene lists for NPC1$^{-/-}$ brain (Supplementary Figure S2A-C) and liver (Supplementary Figure S2D-F) increases robustly (about 5-fold) with disease onset. These results highlight a general trend towards a global down-regulation of mitochondrial genes under chronic lysosomal malfunction.

In order to determine if this effect was specific to mitochondria or also observed in other organelles, we tested how the average expression of peroxisomal-, endoplasmic reticulum- and Golgi-specific genes was affected. The expression of peroxisomal genes was not affected in NPC1$^{-/-}$ brain, but was down-regulated in both asymptomatic and symptomatic NPC1$^{-/-}$ liver (Supplementary Figure S1B). The expression of endoplasmic reticulum-related and Golgi-related genes was not significantly altered (Supplementary Figure S1B). These results suggest that lysosomal stress caused by absence of NPC1 in multiple tissues specifically affects the expression of mitochondrial genes, although disease onset also results in a liver-specific repression of peroxisomal genes.

Figure 1

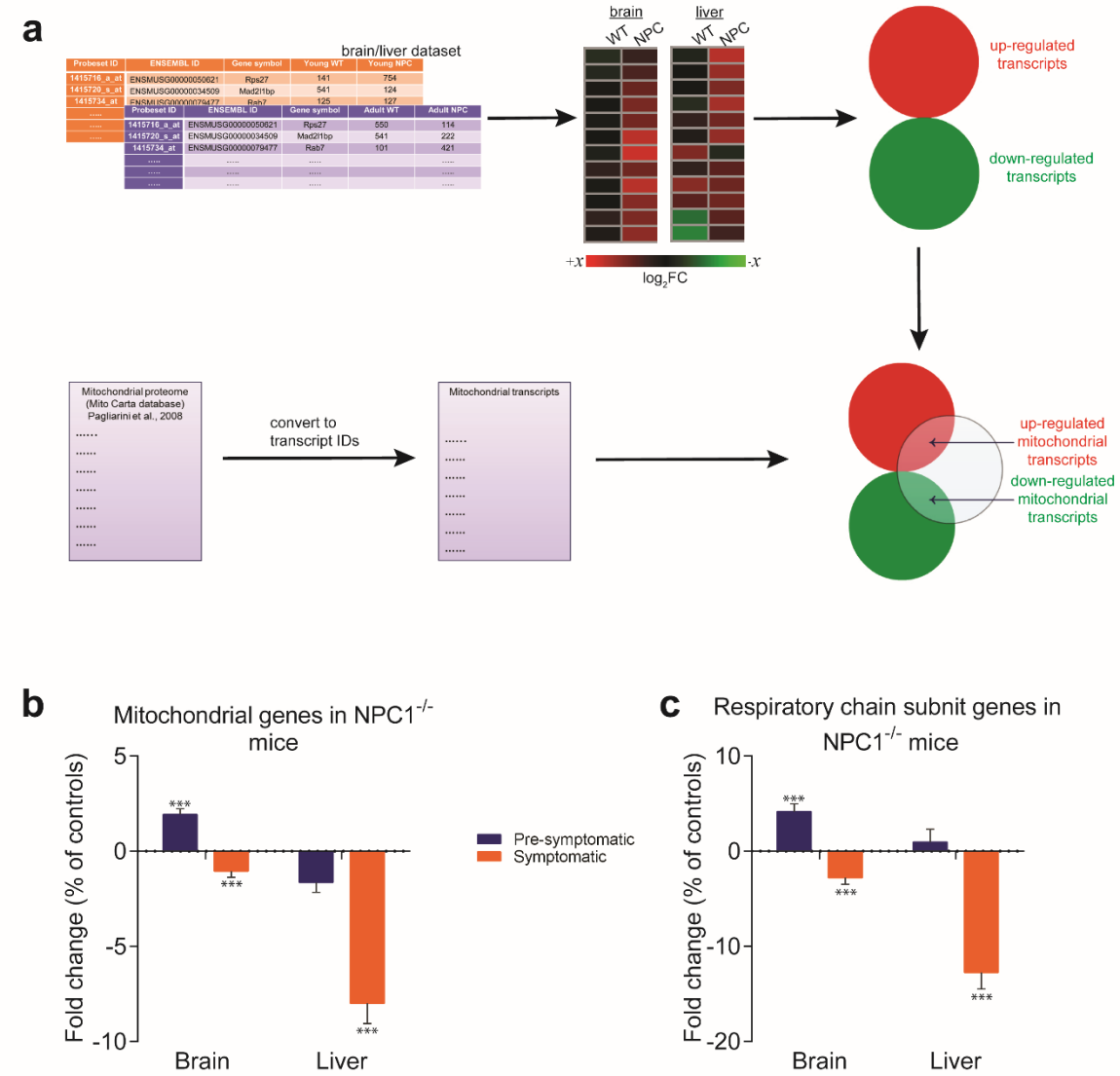

Figure 1. Mitochondria-related genes are down-regulated in brain and liver of symptomatic NPC1$^{-/-}$ mice. (a) Schematic representation of the *in silico* approach. The list of mitochondria-related genes was built by converting the MitoCarta proteome inventory into a transcript list. This was then crossed with the differentially-expressed gene list of brain and liver in symptomatic and asymptomatic NPC-/- versus WT mice. **(b-c)** Decreased expression of genes encoding ~1000 mitochondrial proteins (panel b) and ~100 respiratory chain subunits (panel c) in brain and liver of NPC1$^{-/-}$ mice. The plots (b–c) represent the variation in gene expression comparing the fold change between the average expression in NPC1$^{-/-}$ over NPC$^{+/+}$. This variation is represented as a percentage of the average control expression (e.g., a 20% increase in the mutant mice is shown as 20%, while -25% denotes a 25% decrease). Statistical analyses using *t*-test with Bonferroni correction, adjusted p-values *p<0.05 **p<0.01 ***p<0.001.

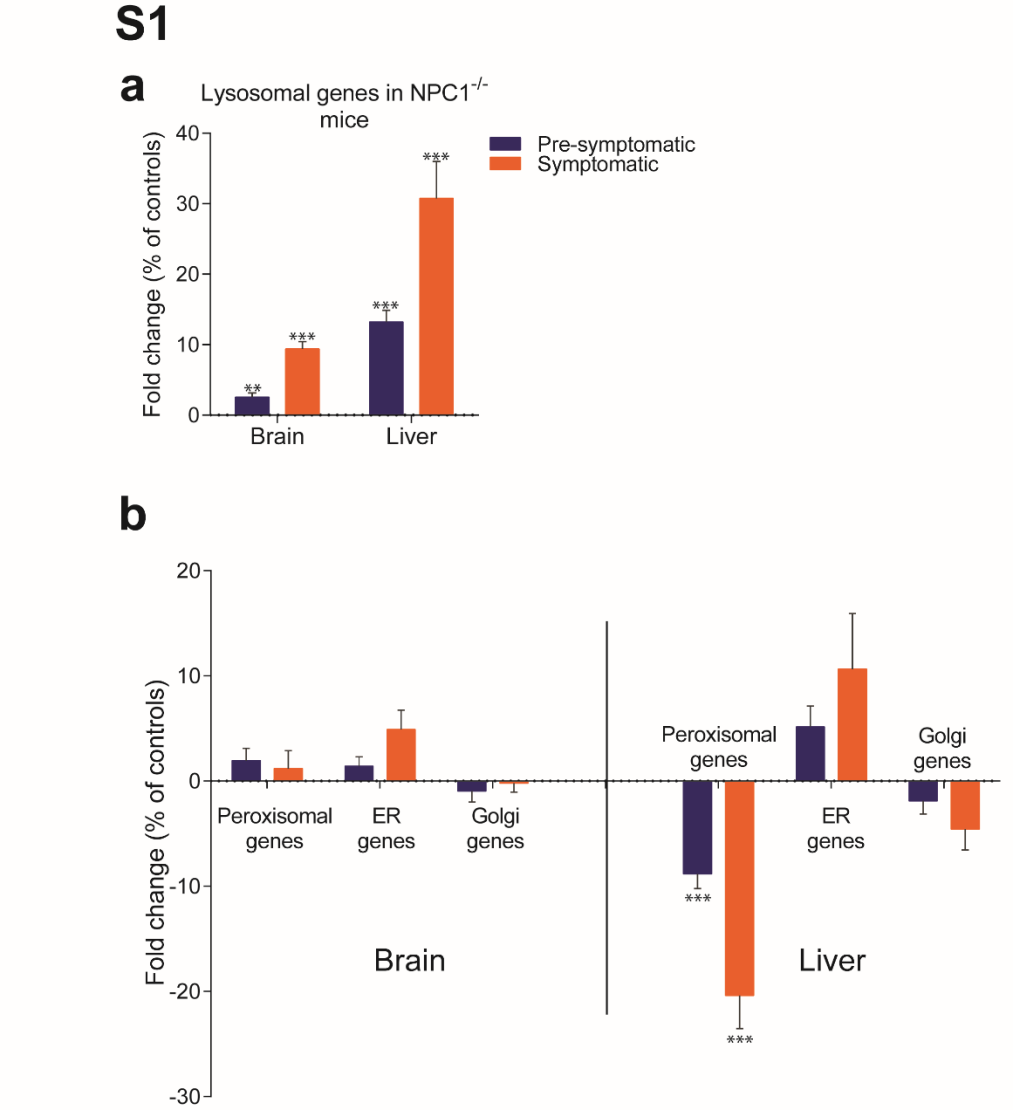

Supplementary Figure 1. Behaviour of organelle-specific gene lists in NPC1-/- tissues. (a) The average expression of 435 lysosomal genes was higher both in brain and liver of NPC1$^{-/-}$, even in asymptomatic mice, and increased further upon disease onset. **(b)** Expression of 86 Golgi-related and 297 endoplasmic reticulum (ER)-related genes did not change significantly between NPC1$^{-/-}$ and WT. Expression of 254 peroxisomal genes was not affected in NPC1$^{-/-}$ brain, but was significantly reduced in asymptomatic NPC1$^{-/-}$ liver and decreased further upon disease onset. The plots represent average fold change±s.e.m. for all genes in the organelle-specific list. T-test p-value (comparing each organelle list in NPC1$^{-/-}$ and WT) with Bonferroni correction, **p<0.01 ***p<0.001

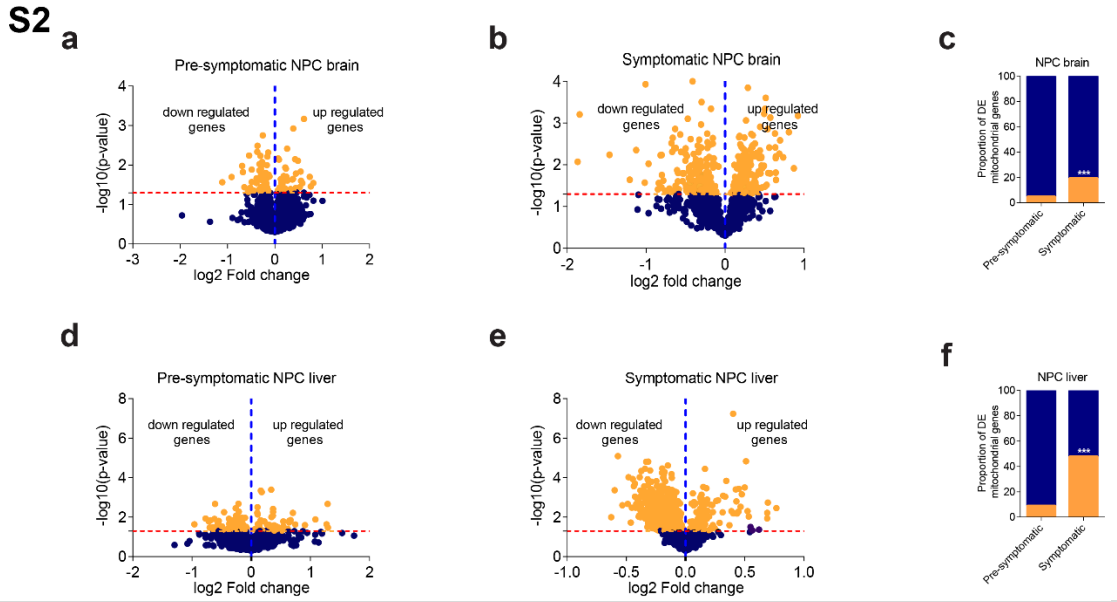

Supplementary Figure 2. Disease progression changes in the expression of mitochondria-related genes in brain and liver of NPC1-/- mice. Of the 1049 mitochondria-related genes analyzed, we determined how many of them were in the differentially-expressed gene (DEG) list of NPC1$^{-/-}$ mice brain and liver. The dot plots show all mitochondria-related genes, with the ones significantly changed between NPC1$^{-/-}$ and WT denoted in yellow. **(a-b)** Volcano plot depicting the fold change and significance p-value of mitochondria-related genes in pre-symptomatic (panel a) and symptomatic (panel b) NPC1$^{-/-}$ brain versus WT. Note the increase in differentially-regulated mitochondrial genes (yellow dots) with the onset of the symptoms. **(c)** Sharp increase (~4-fold) in the proportion of mitochondrial genes that are differentially-regulated in the asymptomatic and symptomatic NPC1$^{-/-}$ brain compared to WT. Fisher exact test p-value ***p<0.001. **(d-e)** Volcano plot depicting the fold change and significance p-value of mitochondria-related genes in pre-symptomatic (panel d) and symptomatic (panel e) NPC1$^{-/-}$ liver versus WT. Note the increase in differentially-regulated mitochondrial genes (yellow dots), mostly in the down-regulated side, with the onset of the symptoms. **(f)** Sharp increase (~5-fold) in the proportion of mitochondrial genes that are differentially-regulated in the asymptomatic and symptomatic NPC1$^{-/-}$ liver compared to WT. Fisher exact test p-value ***p<0.001.

Mitochondrial biogenesis and function are impaired in NPC and ASM patient cells and tissues

To verify the results from the large-scale transcriptional analysis of NPC1$^{-/-}$ tissues, we tested the expression of several genes encoding for mitochondrial proteins in the livers of NPC1$^{-/-}$ mice. The genes tested encode for subunits of the respiratory chain complex I (NDUFS3 and ND6), complex II (SDHA), complex III (CYTB) and complex IV (COX5A, COX1). ND6, CYTB and COX1 are encoded by mtDNA, while all the others are nuclear-encoded. We observed a robust and consistent decrease in the transcript levels of mitochondria-related genes in the livers of NPC1$^{-/-}$ mice (Figure 2A) compared to their respective WT littermates. A similar reduction on the expression of mitochondria-associated genes was also observed in NPC patient fibroblasts (Figure 2B) whose lysosomal phenotype has already been characterized (Kirkegaard et al., 2010).

The accumulation of cholesterol and sphingomyelin in the lysosomes is common to both NPC and acid shingomyelinase (ASM) deficiency (Pentchev et al., 1984; Reagan et al., 2000; Leventhal et al., 2001; Tamura et al., 2006; Lloyd-Evans et al., 2008; Tamasawa et al., 2012; Lee et al., 2013; Platt. 2014). However, while mitochondria in NPC also present increased levels of cholesterol, this does not happen in ASM deficiency (Torres et al., 2017). Since excessive mitochondrial cholesterol can impair mitochondrial function (Torres et al., 2017), we tested if ASM deficiency would also have a repressive effect on mitochondrial biogenesis. Similar to the NPC findings, we observed a decrease in the expression of mitochondria-associated genes in the ASM$^{-/-}$ liver compared to the wt littermates (Figure 2C) as well as in patient fibroblasts of ASM deficiency (Figure 2D).

To assess if this down-regulation of mitochondrial biogenesis in NPC and ASM deficiency had functional consequences for respiratory chain efficiency, we measured the amounts of mitochondrial superoxide, a by-product of the mitochondrial respiratory chain known to be produced in higher amounts when mitochondria are not functioning optimally (Raimundo et al., 2012; Raimundo, 2014), which can be estimated using a superoxide-sensitive

mitochondria-targeted dye, MitoSox. We observed an increase in MitoSox intensity in patient fibroblasts with NPC (Figure 2E) and ASM deficiency (Figure 2F) denoting increased superoxide levels which are indicative of poor mitochondrial performance. Altogether, these results show that the biogenesis of mitochondria is repressed in NPC- and ASM-deficient cells and tissues, and that the existing mitochondria are not functioning optimally. Furthermore, the mitochondrial impairments are likely unrelated to the levels of cholesterol in mitochondria (known to be high in NPC but normal in ASM; Torres et al., 2017), and seem rather a consequence of the lysosomal saturation in NPC and ASM deficiency.

Figure 2

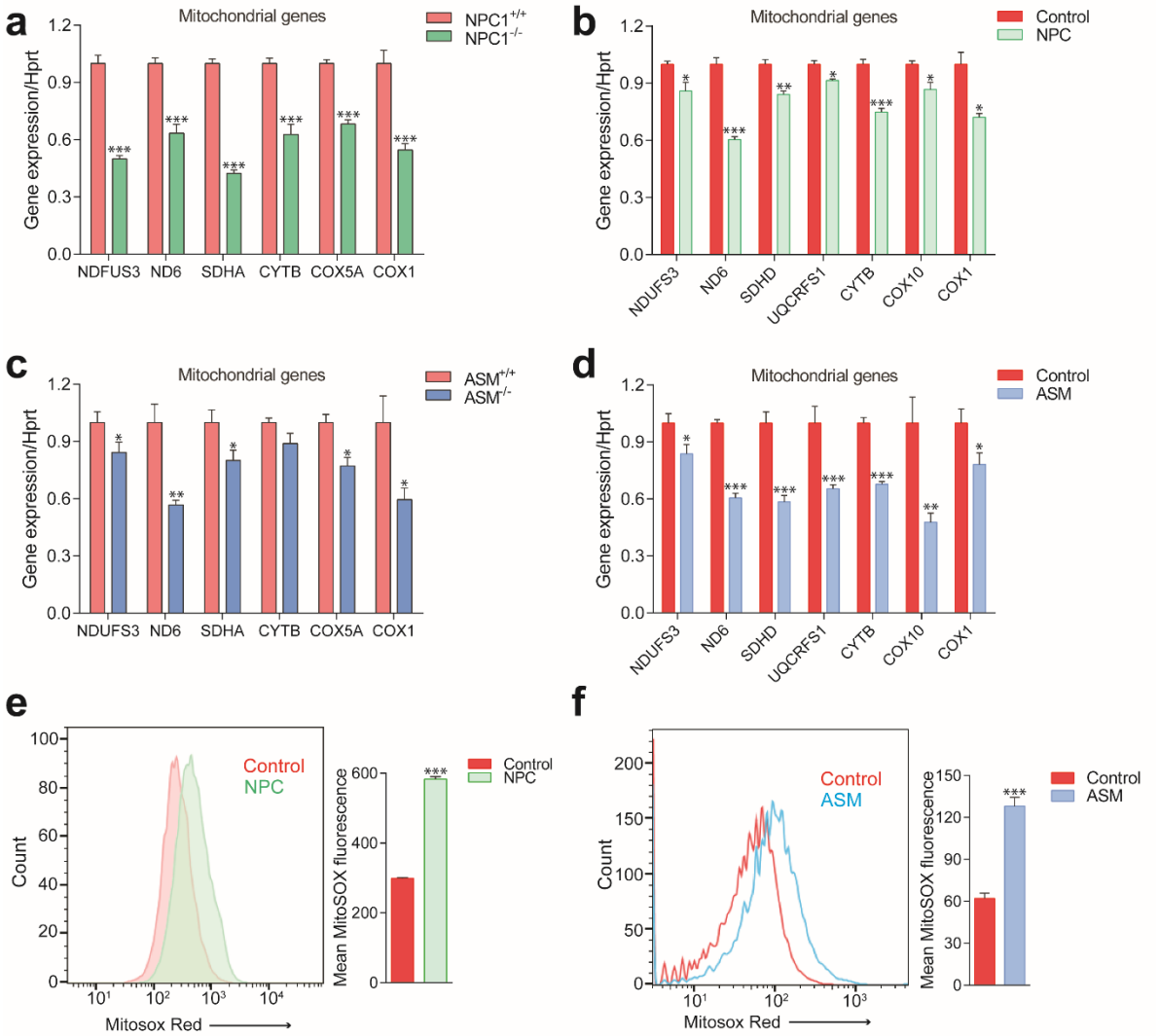

Figure 2. Impaired mitochondrial biogenesis and function in mouse and cellular models of Niemann-Pick disease. The transcript levels of several nuclear-encoded and mitochondrial DNA (mtDNA)-encoded mitochondria-related genes. Transcript levels measured by quantitative PCR (qPCR) by the $\Delta\Delta C_T$ method using HPRT or GAPDH (not shown) as control genes, with three independent replicates per line and two technical replicates for each. **(a)** transcript levels of mitochondria-related genes are decreased in the liver of NPC1 knockout mice ($NPC1^{-/-}$), a model of Niemann-Pick type C. The plot shows average±st.dev.. T-test p-values ***p<0.001, N=8 for each group. Representative experiment shown out of two independent experiments. **(b)** transcript levels of mitochondria-related genes are decreased in the fibroblasts of a patient with compound heterozygote NPC1 mutations (GM18398 Coriell Repository). The plot shows average± st.dev.. T-test p-values *p<0.05 **p<0.01 ***p<0.001. Three independent plates of each line were collected and used for RNA extraction, cDNA synthesis and qPCR. Representative experiment shown out of two independent experiments. **(c)** transcript levels of mitochondria-related genes are decreased in the liver of acid sphingomyelinase knockout ($ASM^{-/-}$) mice, a model of acid sphingomyelinase deficiency. The plot shows average±standard deviation (st.dev.). T-test p-values *p<0.05 **p<0.01, N=6 for each group. Representative experiment shown out of two independent experiments. **(d)** transcript levels of mitochondria-related genes are decreased in fibroblasts from a patient

with acid sphingomyelinase deficiency (only 5% of ASM activity left). The plot shows average±st.dev.. T-test p-values *p<0.05 **p<0.01 ***p<0.001. Three independent plates of each line were collected and used for RNA extraction, cDNA synthesis and qPCR. Representative experiment shown out of two independent experiments. Further characterization of the lysosomal defects in the fibroblasts of this patient are presented in Supplementary Figure 1. **(e-f)** mitochondrial superoxide levels, as assessed by the fluorescence intensity of the superoxide-sensitive mitochondria-targeted dye MitoSox, measured by flow cytometry, are increased in NPC fibroblasts (panel e) and ASM deficient fibroblasts (panel f); representative experiments out of three independent experiments; each experiment had three independent replicates.

Impaired mitochondrial respiration in NPC and ASM deficiency

To further characterize the impact of lysosomal disease on mitochondrial function, we focused on the ASM-deficient fibroblasts, which showed a more robust decrease of mitochondrial biogenesis than NPC and do not have the confounding factor of excessive mitochondrial cholesterol. We used cells from two patients of ASM deficiency, one of which had the lysosomal phenotype already characterized (Corcelle-Termeau et al., 2016). Additionally, we also employed a line from a patient with compound heterozygous loss-of-function mutations in SMPD1 (the gene encoding ASM), which have severe ASM deficiency (5% activity left). The lysosomal impairments in this line have not yet been characterized besides patient diagnosis, therefore we first evaluated lysosomal function in these fibroblasts. One of the consequences of lysosomal dysfunction is the accumulation of autophagic substrates, such as the protein p62 (also known as Sequestosome 1, SQSTM1) as well as autophagosomes (Settembre et al., 2008). We assessed the levels of p62/SQSTM1 and LC3B-II, a marker of autophagosomal mass, by Western blot, and found both sharply increased in the ASM-deficient fibroblasts, as expected (Supplementary Figure S3A). We also assessed the lysosomal proteolytic capacity, by measuring the degradation of the lysosomal substrate DQ-BSA. DQ-BSA is a polymer of fluorescently-tagged bovine serum albumin, which accumulates in the lysosomes. The fluorescence is quenched in the polymeric form and detectable in the monomers. As the lysosomal proteases start cleaving DQ-BSA and releasing monomers, fluorescence starts increasing, and the rate of fluorescence increase is proportional to the activity of lysosomal proteases. We observed a strong decrease in DQ-BSA degradation rate in the ASM fibroblasts (Supplementary Figure S3B). These results support a strong impairment of lysosomal function in ASM-deficient cells used in this study.

We then set to characterize mitochondrial function. First, we monitored the oxygen consumption rate (OCR). This was done with a high-throughput real-time respirometer, which allows the measurement under multiple conditions, such as basal medium, inhibition of

oxidative phosphorylation (when OCR is inhibited) and uncoupled respiratory chain (when OCR occurs unrestrained). We observed a robust decrease in OCR in ASM-deficient fibroblasts which lasted across all conditions tested: basal medium, inhibition of the oxidative phosphorylation with oligomycin, and uncoupling of respiratory chain and oxidative phosphorylation by FCCP (Figure 3A). We determined that the ASM-deficient fibroblasts have 80% decrease in the OCR compared to the control cells in basal conditions (Figure 3B), and about 70% decrease in maximal (uncoupled) conditions (Figure 3B). This result shows a very robust decrease of mitochondrial OCR in ASM-deficient cells. We further observed that the ASM-deficient cells also had a lower amount of TFAM (Figure 3C), a nuclear-encoded protein needed for the stability and transcription of mitochondrial DNA (mtDNA). mtDNA is present at multiple copies per cell, and the copy number is tightly correlated with the amount of TFAM. Accordingly, we find that the mtDNA copy number is decreased in ASM-deficient cells (Figure 3D). These results further support that the ASM-deficient fibroblasts have decreased mitochondrial mass. Overall, ASM-deficient cells present decreased mitochondrial biogenesis, decreased mitochondrial mass and impaired mitochondrial function.

Acid sphingomyelinase generates ceramide, which is itself a powerful signaling lipid, and can be metabolized by acid ceramidase into sphingosine and other signaling lipids. To clarify if the activity of acid ceramidase was affecting the mitochondrial phenotypes observed in ASM-deficiency, we treated control cells with desipramine, a pharmacological inhibitor of both acid sphingomyelinase and acid ceramidase (Zeidan et al, 2006), and measured mitochondrial biogenesis, OCR and superoxide. The transcript levels of mitochondria-related genes were overall down-regulated in desipramine-treated fibroblasts (Suppl. Fig. S4A), which also presented decreased respiratory activity (Suppl. Fig. S4B), with a ~50% decrease in basal OCR and ~60% decrease in uncoupled OCR (Suppl. Fig. S4C). An increase in the levels of superoxide was also observed (Suppl. Fig. S4D).

Since one of the known consequences of ASM deficiency is accumulation of cholesterol in the lysosomes (Lloyd-Evans et al., 2008; Oninla et al., 2014), and given that we observed

similar perturbations on mitochondrial homeostasis in ASM- and NPC-deficient patient fibroblasts, we tested if pharmacological inhibition of NPC1 would also be sufficient to impact mitochondrial biogenesis and function. We treated control cells with the NPC1 inhibitor U18666A (Lu et al., 2015), and observed decreased expression of mitochondria-associated genes (Supplementary Figure S5A), lower respiration (Suppl. Fig. S5B) with ~30% lower basal OCR and ~50% lower uncoupled OCR (Suppl. Fig. S5C). Finally, the treatment with U18666A resulted in increased superoxide levels (Suppl. Fig. S5D). Thus, pharmacological inhibition of ASM or NPC1, resulting in both cases in accumulation of lysosomal sphingomyelin and cholesterol, is sufficient to cause decreased expression of mitochondrial genes and impaired mitochondrial respiratory chain activity. This effect seems to be independent of acid ceramidase activity.

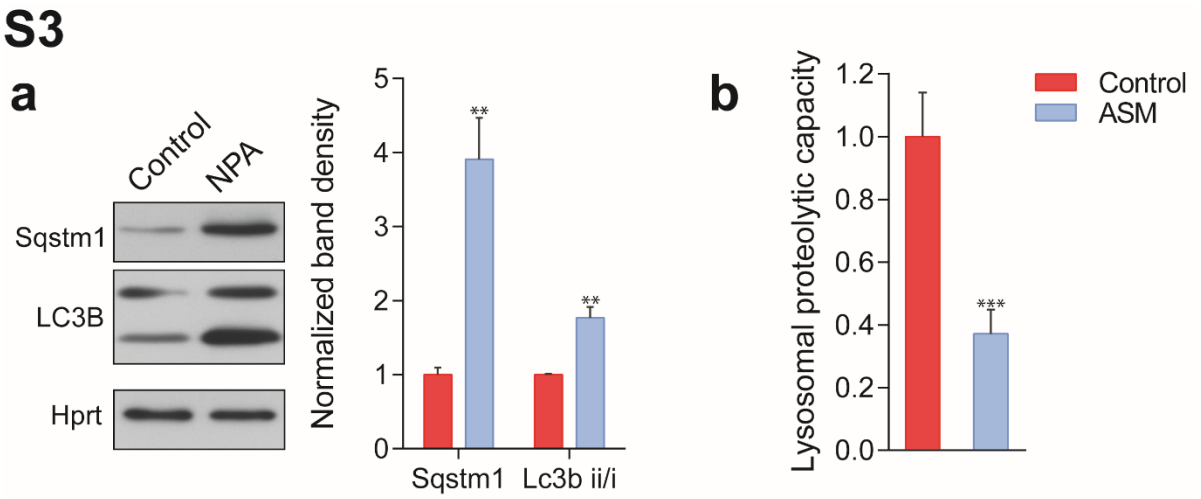

Supplementary Figure 3. Validation of lysosomal defects in patient fibroblasts. The ASM-deficient cells used in this manuscript have 5% left of acid sphingomyelinase activity, and present the expected signs of lysosomal impairment, specifically **(a)** decreased autophagic capacity with accumulation of autophagic substrates (p62 also known as Sequestosome 1, Sqstm1) and autophagosomes, as assessed by the autophagosomal marker LC3B-II, and **(b)** decreased lysosomal proteolytic capacity, as assessed by the rate of DQ-BSA degradation by the lysosomal proteases in whole cells.

Figure 3

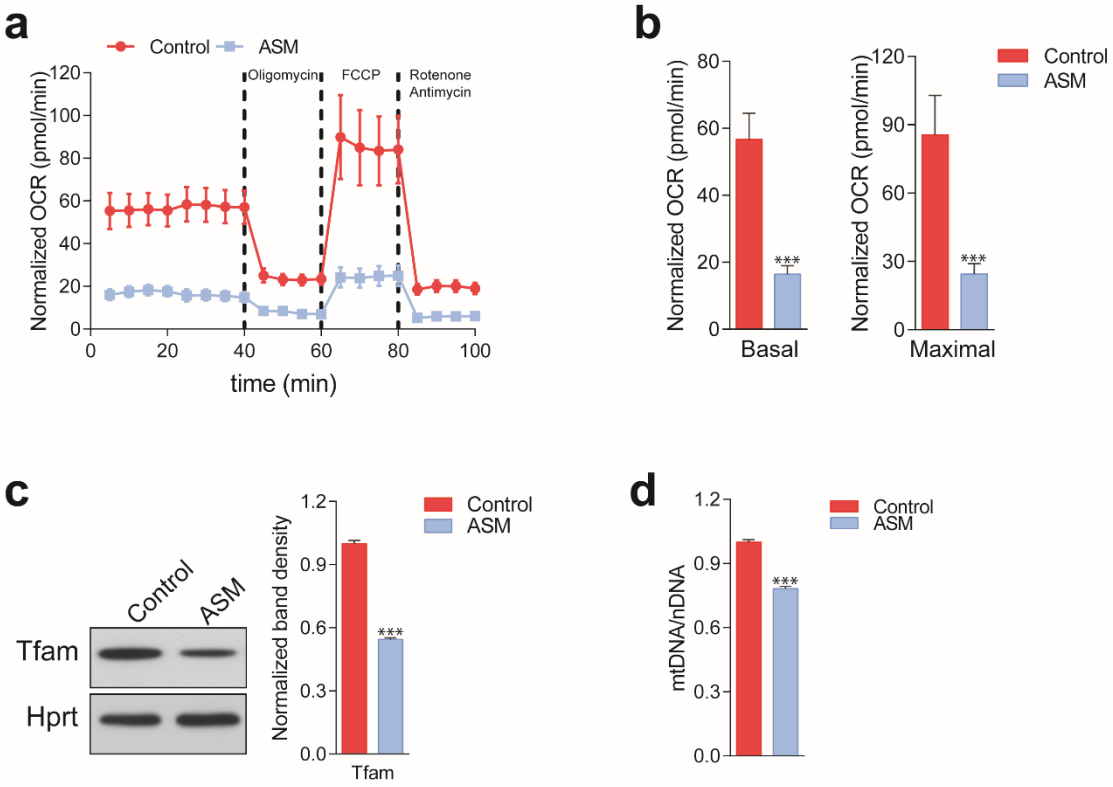

Figure 3. Mitochondrial function and mitochondrial mass are impaired in acid sphingomyelinase (ASM)-deficient patient fibroblasts.
(a) ASM-deficient fibroblasts have substantially lower O_2 Consumption Rate (OCR) than controls. OCR was measured using whole cells, sequentially in basal conditions (complete medium), after oxidative phosphorylation inhibition using the ATPase inhibitor oligomycin, after uncouling the respiratory chain from oxidative phosphorylation using the uncoupler FCCP, and after inhibition of the respiratory chain using complex I inhibitor rotenone and

complex III inhibitor antimycin. The measurements were made in a 96-well plate using a SeaHorse Extracellular Flux analyser. The average±standard error of the mean (s.e.m.) of at least eight wells per cell line is plotted over time. OCR was normalized to the amount of protein in each well. The plot shows a representative experiment of three independent experiments. **(b)** Reduced basal and maximal (uncoupled) OCR in ASM-deficient fibroblasts quantified from the curves in (a). Representative experiment with eight replicates for each cell line. At least three independent experiments were performed. T-test p-value ***p<0.001. **(c)** Western blot analysis of whole cell extracts showing decreased amounts of the mitochondrial protein TFAM in ASM-deficient fibroblasts compared to controls. HPRT was used as a loading control. The quantification of three independent experiments is plotted on the right side as average±st.dev. T-test p-value ***p<0.001 **(d)**

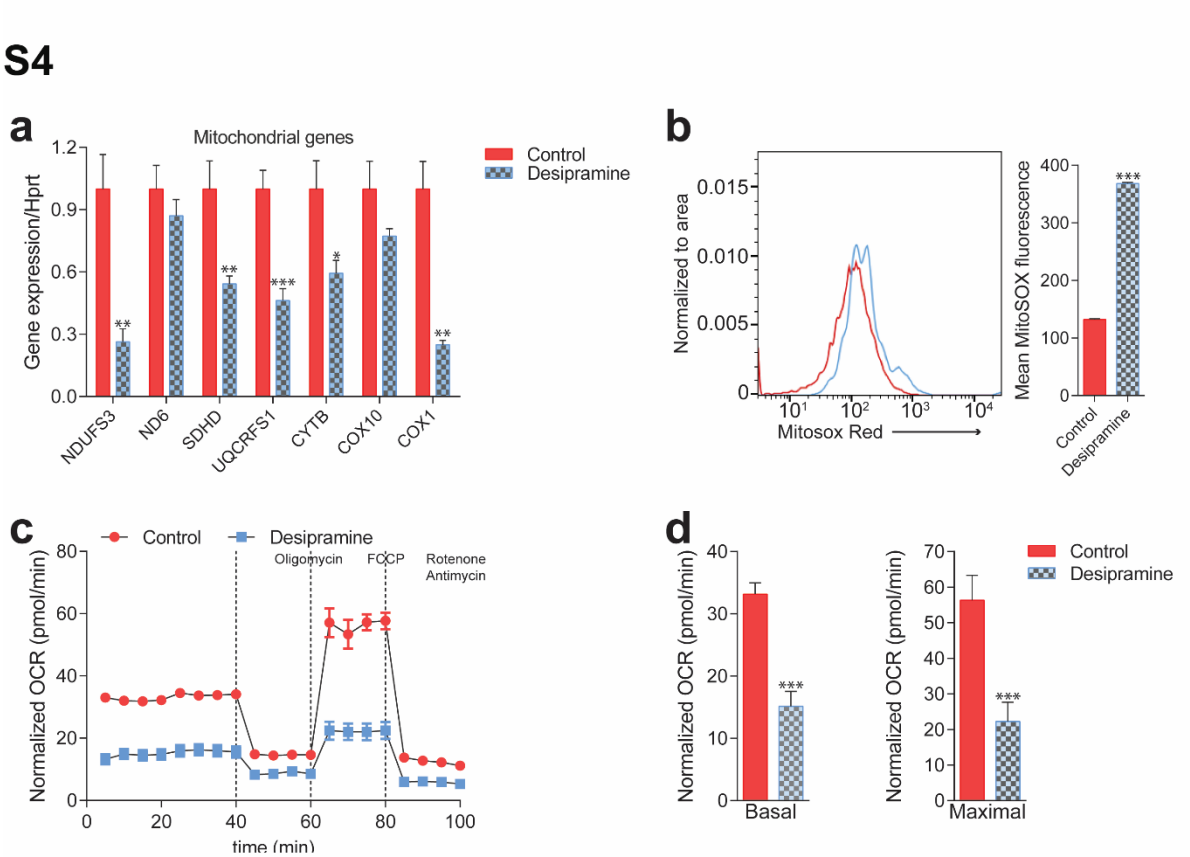

Supplementary Figure 4. Mitochondrial deficits in control fibroblasts treated with desipramine 40μM for 72h (inhibitor of acid sphingomyelinase).
(a) Transcript levels of mitochondria-related proteins are decreased in desipramine-treated fibroblasts (average±st.dev., N=3, representative experiment repeated twice). T-test p-values *p<0.05 **p<0.01 ***p<0.001. Sterile distilled water used as vehicle control. **(b)** Increased mitochondrial superoxide levels, as assessed by MitoSox intensity, in desipramine-treated cells (DMSO as vehicle control), measured by flow cytometry. The plot shows the average±st.dev. of a representative experiment with three independent samples, repeated twice. T-test p-values ***p<0.001 **(c-d)** Decreased O2 consumption rate (OCR) in desipramine-treated fibroblasts under the indicated conditions, quantified in panel d (average±s.e.m. of at least eight independent replicates, repeated twice). Sterile distilled water used as vehicle control.

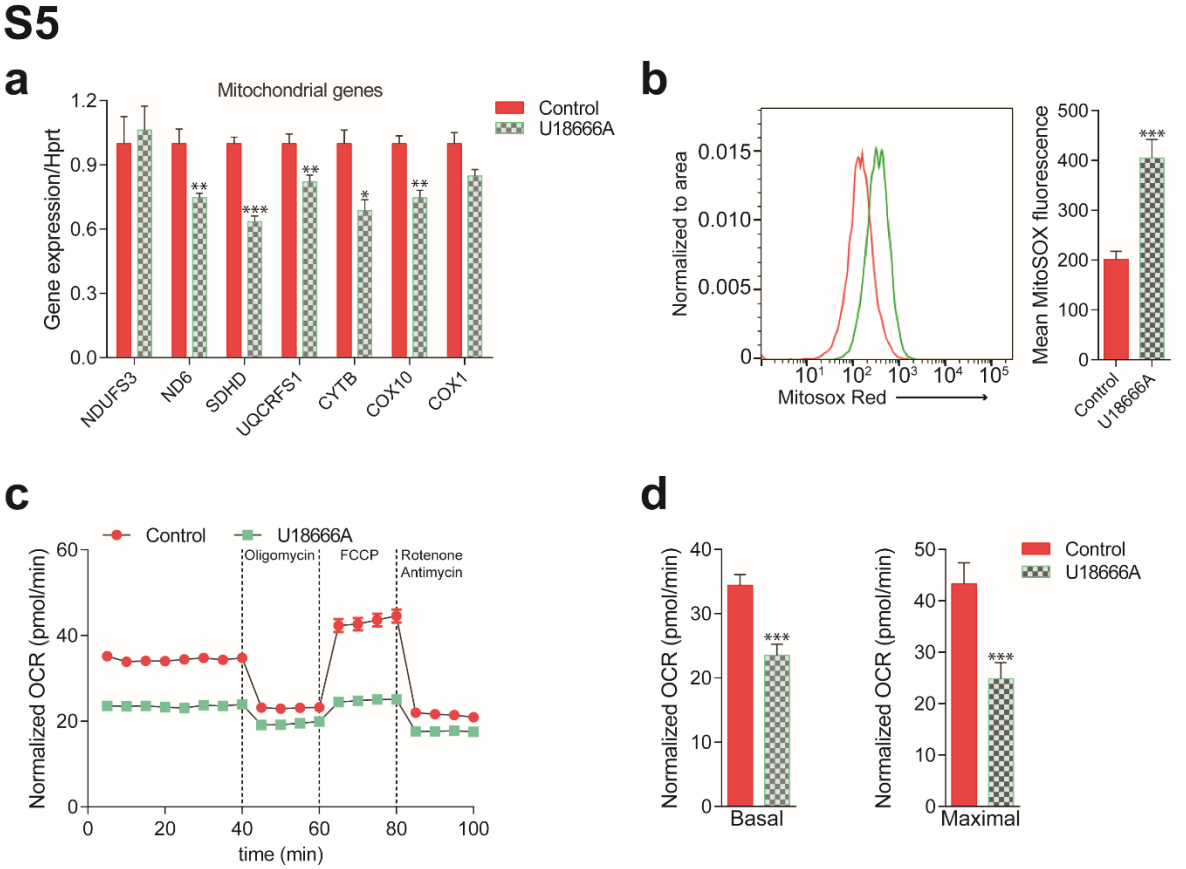

Supplementary Figure 5. Mitochondrial deficits in control fibroblasts treated with U18666A 10μM for 72h (inhibitor of NPC1).
(a) Transcript levels of mitochondria-related proteins are decreased in U18666A-treated fibroblasts (average±st.dev., N=3, representative experiment repeated twice). T-test p-values *p<0.05 **p<0.01 ***p<0.001. DMSO used as vehicle control. **(b)** Increased mitochondrial superoxide levels, as assessed by MitoSox intensity, in U18666A-treated cells (DMSO as vehicle control), measured by flow cytometry. The plot shows the average±st.dev. of a representative experiment with three independent samples, repeated twice. T-test p-values ***p<0.001 **(c-d)** Decreased O2 consumption rate (OCR) in U18666A-treated fibroblasts under the indicated conditions, quantified in panel f (average±s.e.m. of at least eight independent replicates, repeated twice). DMSO used as vehicle control.

KLF2 and ETV1 are up-regulated in NPC1$^{-/-}$ tissues and repress transcription of mitochondria-associated genes

Having established a clear mitochondrial phenotype in NPC and ASM deficiency, we set out to identify the underlying mechanism. The robust decrease in the expression of hundreds of mitochondria-related genes in NPC1$^{-/-}$ brain (Suppl. Figure S1C) and NPC1$^{-/-}$ liver (Suppl. Figure S1F) suggests the involvement of a coordinated transcriptional program, and therefore of transcriptional regulators, such as transcription factors. To determine which transcription factors might be mediating the repression of mitochondria-associated genes, we took an unbiased bottom-up approach to determine potential transcriptional regulators. Given that the whole mitochondrial gene list has ~1000 genes, we focused on the RC/OXPHOS list, which shows the same behavior as the complete mitochondrial gene list (as shown in Figures 1 and Suppl. Figure S2) and has a more manageable size (~100 genes). Using the Genomatix Gene2Promoter tool, we obtained the genomic sequences (Mus musculus) of the promoter regions of the RC/OXPHOS genes, from -500 base pairs upstream the transcription start site, to +100 base pairs downstream. This region is sufficient to account for the regulation of gene expression by transcription factors in many promoters of mitochondrial genes (Gleyzer et al., 2005; Virbasius and Scarpulla, 1994). We then used Genomatix Matinspector tool to analyze the gene promoters for transcription factor binding sites (cis-elements), and identified those statistically enriched (illustrated in Figure 4A). The most overrepresented cis-elements in the promoters of RC/OXPHOS genes are the transcription factor families SP1, E2F, Krueppel-like factors (KLF) and ETS factors (Table II). In parallel, as control, we carried out a similar approach for the lysosomal gene list (whose expression is increased, in contrast with the mitochondrial genes) and observed that the SP1 and E2F families were also significantly enriched in the promoters of lysosomal genes (Supplementary Table I). Given that the expression of lysosomal genes and mitochondrial genes is affected in opposite ways, we reasoned that it would be unlikely that the same transcription factors were driving two opposite processes. For this reason, we proceeded only with the KLF and ETS families, which only scored as significantly enriched in the mitochondrial promoters (Table II).

Next, we again resorted to the transcriptome dataset of NPC1$^{-/-}$ brain and liver to determine if any transcription factors in the KLF2 and ETS families were predicted to have increased or decreased activity during NPC disease progression. Using Ingenuity Pathway Analysis, we determined which transcription factors scored as significant regulators in these tissues (Supplementary Table II). The only transcription factor of the KLF family meeting the criteria was KLF2. Several ETS family transcription factors have redundant binding sites (Hollenhorst et al., 2007), so we tested the three members that scored in the Genomatix promoter analysis, SPI1, ELK1 and ETV1. SPI1 is expressed in macrophages and not expressed in fibroblasts (Feng et al., 2008; Suzuki et al., 2012), and accordingly we could not detect the expression of SPI1 in control or patient fibroblasts, either at transcript or protein (data not shown). While ELK1 was not changed at transcript level (Supplementary Figure S6A), ETV1 was significantly increased in ASM deficiency patient fibroblasts (Supplementary Figure S6A). The transcript levels of KLF2 were not changed in ASM deficiency (Supplementary Figure S6B).

We then focused on KLF2 and ETV1 (Figure 4A). First, we tested if the levels of these proteins were affected in NPC- or ASM-deficient fibroblasts, by Western blotting, and found that both KLF2 and ETV1 were robustly up-regulated in both conditions, including the in-house as well as the previously characterized ASM-deficient line (Figure 4B). We again compared the ASM-deficient fibroblasts with control fibroblasts treated with the inhibitor of both ASM and acid ceramidase. Desipramine-treated fibroblasts yielded a similar result: both KLF2 and ETV1 are up-regulated at protein level (Supplementary Figure S7A, quantified in S7B) but only ETV1 transcript levels are significantly changed (Supplementary Figure S7C). Altogether, these results suggest that the accumulation of KLF2 in response to lysosomal lipid storage is regulated post-translationally, while ETV1 is regulated at transcript level.

Given that ETV1 and KLF2 are predicted by our promoter analysis to have binding sites in the promoters of the genes encoding for respiratory chain subunits, and that increased expression of these two transcription factors correlates with repression of respiratory chain

genes, we reasoned that KLF2 and ETV1 might be mediating this repression. To explore this possibility, we took advantage of another publicly available transcriptome dataset of erythroid cells of KLF2$^{-/-}$ and WT mice (GSE27602). We observed an increase in the average transcript levels of the "mitochondria gene list" in the KLF2$^{-/-}$ cells compared to the WT littermates (Supplementary Figure S8). The effect is also observed, with higher magnitude, when measuring the average expression of the genes encoding for respiratory chain subunits (Supplementary Figure S8). These results suggest that KLF2 is able to repress mitochondrial biogenesis *in vivo*. In addition, it is noteworthy that several known ETV1 targets are mitochondrial genes, as previously shown by chromatin immunoprecipitation (Baena et al., 2013) and illustrated in Supplementary Figure 9. To test the effect of ETV1 on the expression of mitochondria-related genes, we expressed full length ETV1 (ETV1^{FL}) as well as ETV1 lacking the DNA-binding domain (ETV1$^{1-334}$) in control fibroblasts (Figure 4C) and evaluated the effect on the expression of mitochondria-related genes. The overexpression of ETV1^{FL} elicited a decrease in the transcript levels of most mitochondria-associated genes (Figure 4D). However, ETV1$^{1-334}$ did not repress the transcript levels of these mitochondrial-related genes. This result is coherent with the role of ETV1 as a repressor of mitochondrial biogenesis, and further demonstrates that this repression occurs via direct binding of ETV1 to DNA (Janknecht, 1996), thus validating our *in silico* promoter analysis. The unexpected increase in the transcript levels of mitochondria-related genes under overexpression of ETV1$^{1-334}$, unable to bind DNA, may be explained by ETV1 functioning as a homodimer (Poon, 2012). Therefore, overexpression of a mutant unable to bind DNA might titrate out the wild-type ETV1, thus effectively functioning as a dominant-negative ETV1 isoform, with the consequent activation of mitochondrial biogenesis.

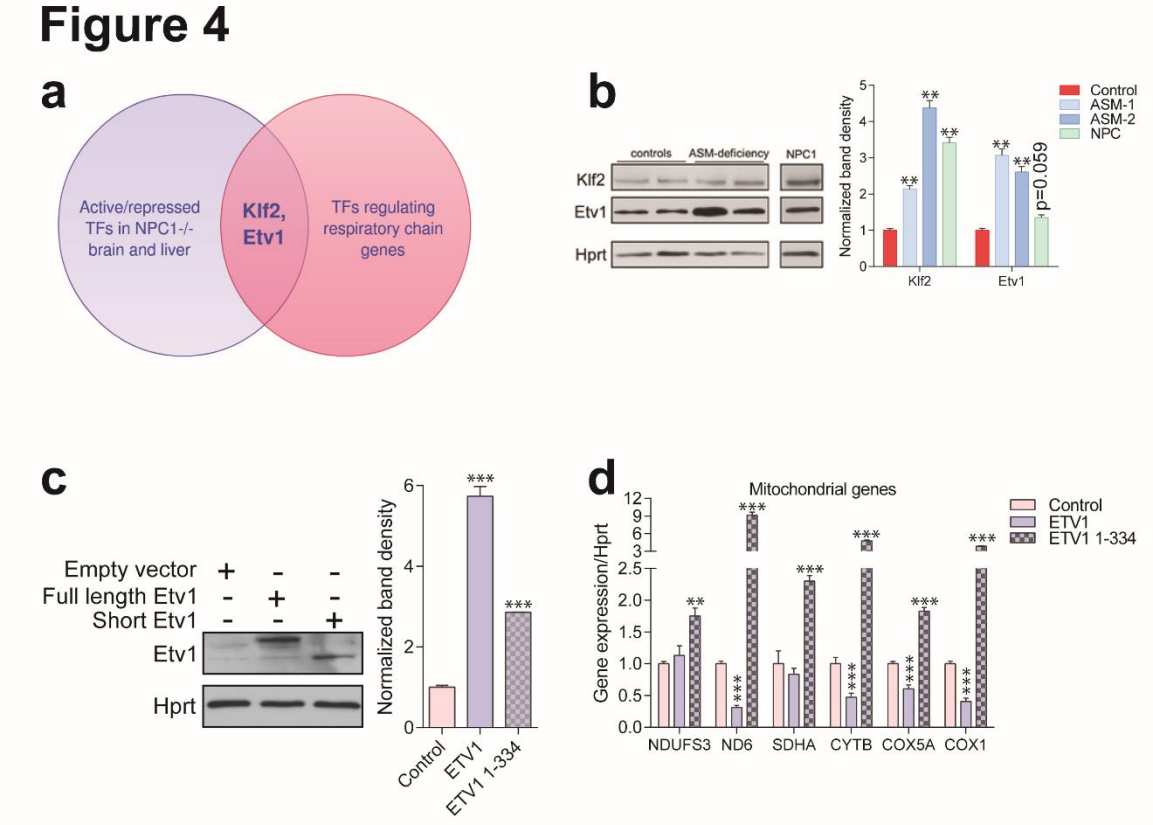

Figure 4. Transcription factors Etv1 and Klf2 are induced in Niemann-Pick and involved in the regulation of mitochondrial biogenesis.
(a) Schematic representation of the intersection between the list of transcription factors (TFs) that are significantly activated or repressed in tissues of NPC1-/- mice, and the list of TFs that are predicted to regulate the expression of mitochondrial respiratory chain genes, which yields KLF2 and ETV1 as hits. **(b)** Increased Klf2 and Etv1 protein levels in ASM-deficient (both the in-house line, lane 3, as well as the Coriel line, lane 4) and NPC fibroblasts, shown in a representative (out of three independent experiments) western blot of whole cell extracts, with quantification (average±st.dev. of at least three independent experiments) of band densities in the adjacent plot. T-test p-values **p<0.01 ***p<0.001 **(c)** Overexpression of $ETV1^{WT}$ (full length ETV1) and of $ETV1^{1-334}$, lacking the C-terminus which includes the DNA-binding domain. Representative western blot, quantification of band densities from two independent experiments with two technical replicates each on the right panel (average±st.dev.) **(d)** Overexpression of $ETV1^{WT}$ significantly down-regulates the transcript levels of most mitochondria-related genes, while ETV11-334, unable to bind DNA, causes an increase in transcript levels. Transcript levels measured by quantitative PCR (qPCR) by the $\Delta\Delta C_T$ method using HPRT or GAPDH (not shown) as control genes, with three independent replicates per line and two technical replicates for each. The plot shows average±st.dev., T-test p-values **p<0.01 ***p<0.001, two independent experiments with three replicates each.

S6

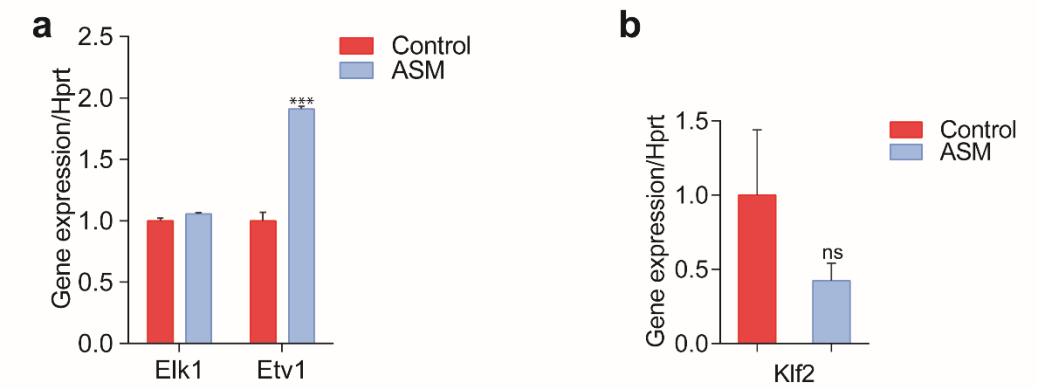

Supplementary Figure 6. Etv1 and Klf2 transcript levels in acid sphingomyelinase-deficient fibroblasts. (a) Transcript levels of ETS family members Elk1 and ETV1 in ASM-deficient fibroblasts, measured by qPCR as described above. Average±st.dev. of three independent samples repeated twice. (b) Transcript levels of KLF2 in ASM-deficient fibroblasts, measured by qPCR as described above. Average±st.dev. of three independent samples repeated twice.

S7

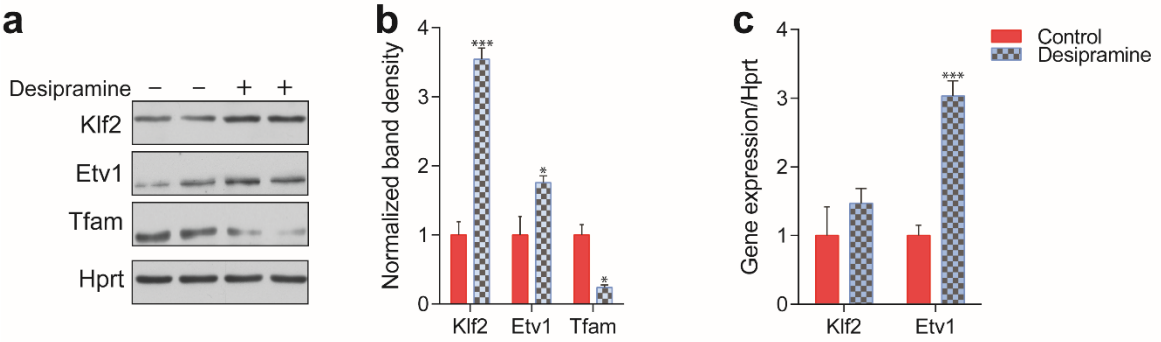

Supplementary Figure 7. Etv1 and Klf2 levels in desipramine-treated fibroblasts. (a) KLF2 and ETV1 protein levels are increased and mitochondrial protein TFAM is reduced in desipramine-treated fibroblasts, as assessed by western blot. **(b)** Quantification of the western blot shows average±st.dev. of two experiments with two replicates each. T-test p-value *p<0.05 ***p<0.001 **(c)** Transcript level of KLF2 is not changed and ETV1 is increased in desipramine-treated fibroblasts, as measured by qPCR as described above. Quantification shows average±st.dev. of three independent samples repeated twice. T-test p-value ***p<0.001

S8

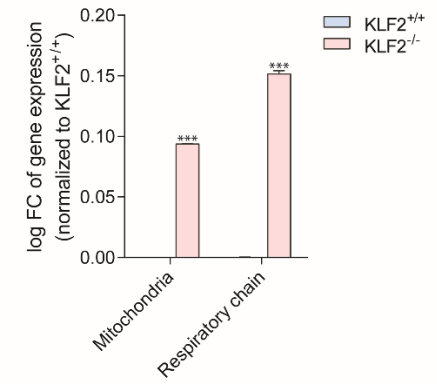

Supplementary Figure 8. Increased expression of mitochondria-related genes in the absence of KLF2. Using a publicly-available transcriptional dataset of erythroid cells obtained from KLF2-/- and WT mice, we found that the average expression of ~1000 mitochondria-related genes is increased ~10% in KLF2-/-, while the expression of ~100 respiratory chain subunits is increased ~15% in KLF2-/-. These results support a repressive role of KLF2 on mitochondrial biogenesis. Plot shows average±s.e.m. of fold change of all genes in the gene list. T-test with Bonferroni correction ***p<0.001

S9

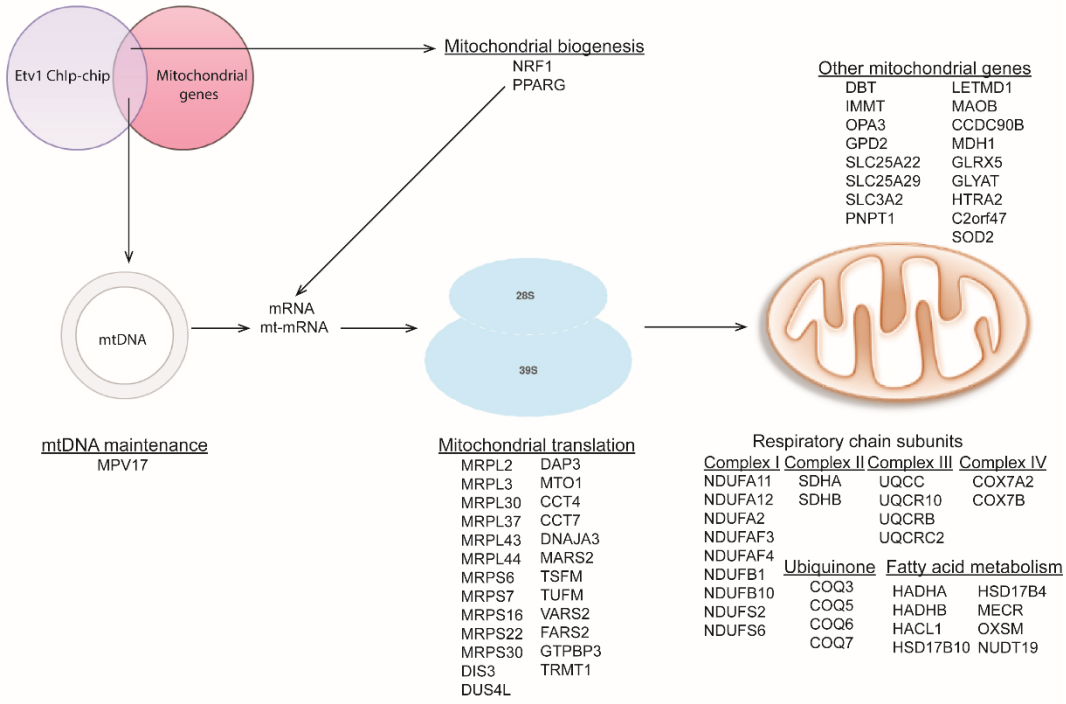

Supplementary Figure 9. Targets of Etv1 as determined by ChIpSeq data analysis. Graphic representation of publicly available Etv1 ChIpSeq data, highlighting how many of its target genes encode proteins involved in different aspects of mitochondrial function.

Silencing of KLF2 and ETV1 in ASM deficiency rescues mitochondrial biogenesis and function

To test if KLF2 and ETV1 were indeed repressing mitochondrial biogenesis in ASM-deficient cells, we knocked-down ETV1 (Figure 5A) and KLF2 (Figure 5B), independently, in ASM-deficient fibroblasts. Both knock-downs were effective (Figures 5A-B), and both resulted in an increase of mitochondrial protein levels back to control levels, as exemplified for TFAM (Figures 5A-B). Interestingly, transcription factor nuclear respiratory factor 1 (NRF1), a known inducer of mitochondria-related gene expression, was also sharply down-regulated in ASM-deficient fibroblasts, and was rescued by the silencing of ETV1 or of KLF2. This result suggests a compound effect of repression of mitochondria-related genes by KLF2 and ETV1, combined with decreased activation of the expression of the same genes by NRF1. Notably, the transcript levels of mitochondria-associated genes, which are down-regulated in ASM-deficient fibroblasts, were increased by the silencing of ETV1 and even more robustly increased by KLF2 silencing (Figure 5C). This includes NRF1 and its closely related protein nuclear respiratory factor 2 (NRF2, also known as GABPA), again suggesting that these two transcription factors may be repressed by KLF2 and ETV1. Importantly, the improvement in the expression of mitochondria-associated genes by silencing KLF2 or ETV1 is not due to an improvement of the lysosomal phenotype. We measured readouts of lysosomal function such as the accumulation of autophagosomal marker LC3BII or autophagy substrate p62, by Western blot, and found that silencing of KLF2 or ETV1 had no impact on the lysosomal dysfunction in ASM-deficient cells (Supplementary Figure S10A-B). Finally, mitochondrial respiration was partly rescued in ASM-deficient fibroblasts by the knock-down of ETV1 and robustly rescued by KLF2 silencing (Figure 5D). Altogether, these results show that KLF2 and ETV1, two transcription factors that are increased in ASM and NPC deficient fibroblasts and hyperactive in NPC1-/- tissues, repress mitochondrial biogenesis and that their silencing restores mitochondrial biogenesis and function in ASM fibroblasts.

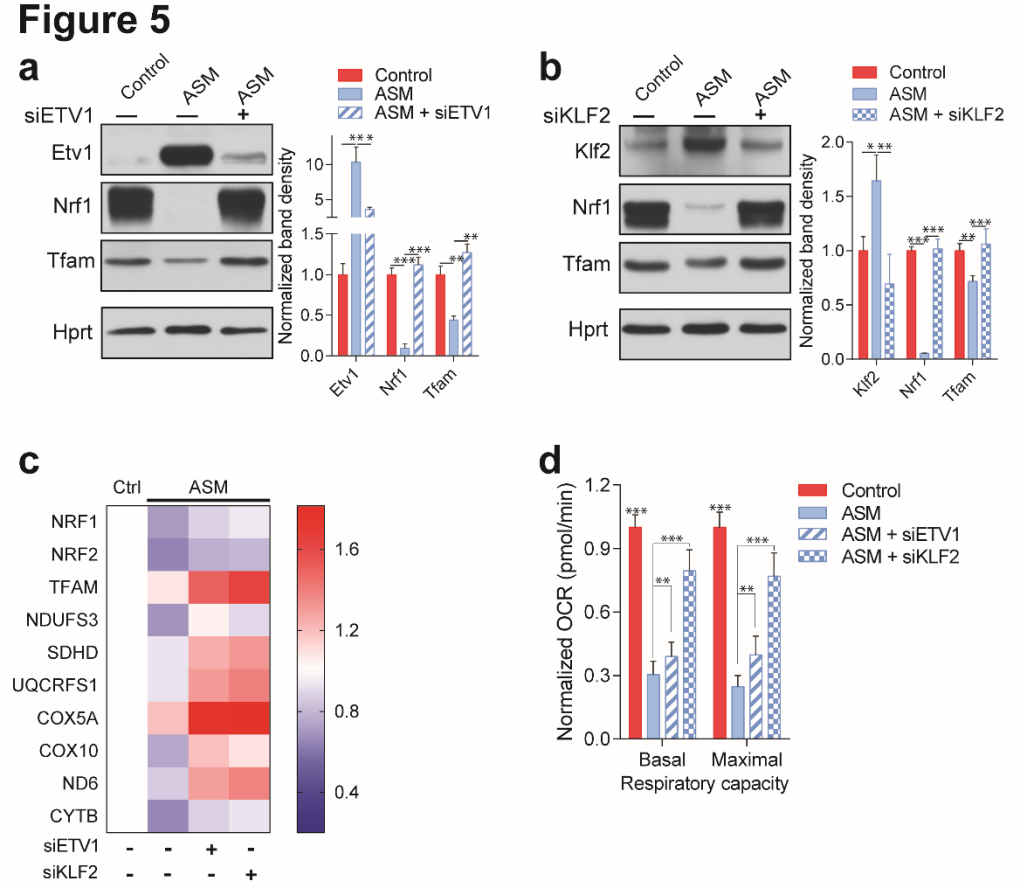

Figure 5. Silencing of ETV1 or KLF2 rescues mitochondrial biogenesis and function in Niemann-Pick fibroblasts. Using siRNA-mediated silencing, we knocked-down Etv1 **(a)** or Klf2 **(b)** in ASM-deficient fibroblasts, which brought the protein levels of mitochondrial protein TFAM and of mitochondrial biogenesis regulator NRF1 to control levels, as shown in a representative (out of three independent experiments) western blot of whole cell extracts, with quantification of band densities in the adjacent plots (average±st.dev.). Scrambled siRNA was used as control in both control and ASM-deficient cells for all experiments involving ETV1 or KLF2 silencing. T-test p-values **p<0.01 ***p<0.001 **(b)** Silencing of ETV1 or KLF2 increases the transcript levels of mitochondrial genes, as assessed by qPCR. The data is presented in a heatmap, in which blue denotes decrease in expression compared to the control cells (white represents no change relative to the control values) and red denotes increase. Note the mostly decreased (blue) mitochondrial genes in NP and their turn to red (increased expression) when ETV1 or KLF2 are silenced. **(f)** Silencing of ETV1 or KLF2 in ASM-deficient cells increases OCR, as measured by real-time respirometry using the SeaHorse Extracellular Flux analyzer. The plot shows the average±s.e.m. of eight technical replicates per condition. T-test p-values **p<0.01 ***p<0.001

S10

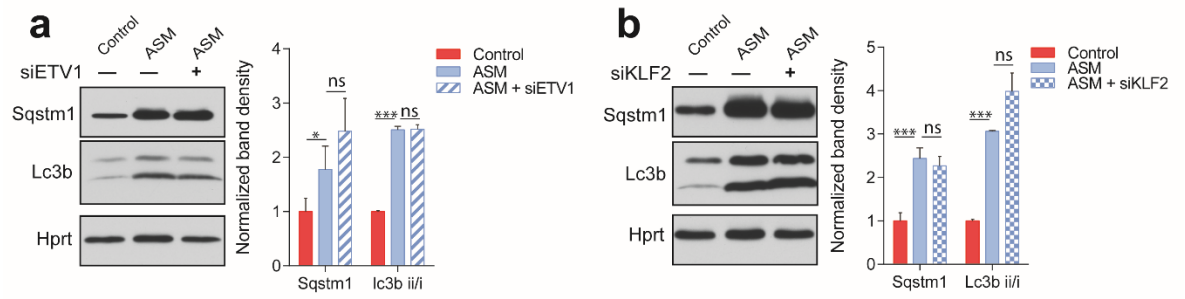

Supplementary Figure 10. Autophagy defects in Niemann Pick patients are independent of Klf2 and Etv1. To assess if silencing of ETV1 or KLF2 in ASM-deficient fibroblasts had any impact on lysosomal function, we assessed the accumulation of autophagic substrates p62 (Sqstm1) and LC3BII, a marker of autophagosomes. No effect on these parameters was observed when ETV1 (panel a) or KLF2 (panel b) were silenced, as assessed by western blot. Quantification shows the average±st.dev of two independent experiments. T-test p-value *p<0.01 ***p<0.001; ns, non-significant.

KLF2 regulates ETV1 in an ERK-dependent manner

The silencing of KLF2 had a more robust effect on the recovery of mitochondrial function than the silencing of ETV1. For this reason, we set to understand if these transcritption factors work in parallel pathways or if they are epistatic. First, we checked if these two transcription factors were epistatic, and observed that the silencing of KLF2 in ASM-deficient fibroblasts results in the ablation of ETV1 (Figure 6A). ETV1 silencing has no effect on KLF2 (Figure 6A). Since we have shown above that ETV1 is regulated at transcript level, this result implies that KLF2 regulates (activates) the transcription of the gene encoding ETV1, in agreement with the increased transcript levels of ETV1 in ASM-deficient fibroblasts.

Next, we tested known signaling modulators of KLF2 or ETV1 in ASM-deficient fibroblasts. Akt signaling down-regulates KLF2 (Skon et al., 2013), and we observed that Akt seems deactivated in ASM-deficient fibroblasts, as assessed by decreased phosphorylation of Akt Serine 473 (Figure 6B). ERK is a positive effector of ETV1 (Janknecht, 1996), and we found ERK signaling increased in ASM-deficient fibroblasts (Figure 6B). mTORC1 signaling is often involved in lysosomal stress signaling, and we found it activated in ASM-deficient fibroblasts, as assessed by the phosphorylation of p70S6 kinase (P70S6K) Threonine 389 (Figure 6B). AMPK signaling, which regulates mTORC1 as well as biogenesis of mitochondria and lysosomes, was not affected, as assessed by phosphorylation of acetyl-CoA carboxylase (ACC) (Figure 6B). Inhibition of mTORC1 signaling in ASM-deficient fibroblasts by treatment with the mTORC1 inhibitor torin1 had no effect on the expression of mitochondria-related genes or mitochondrial function (data not shown).

We next tested if the activation of ERK signaling was related to the increased levels of ETV1. We treated the ASM-deficient fibroblasts with the ERK inhibitor U0126, which led to the ablation of ERK signaling, as expected (Figure 6C). KLF2 was mostly unaffected by ERK inhibition (Figure 6C). However, ETV1 was returned to control levels (Figure 6C), suggesting that induction of ETV1 by KLF2 requires active ERK signaling.

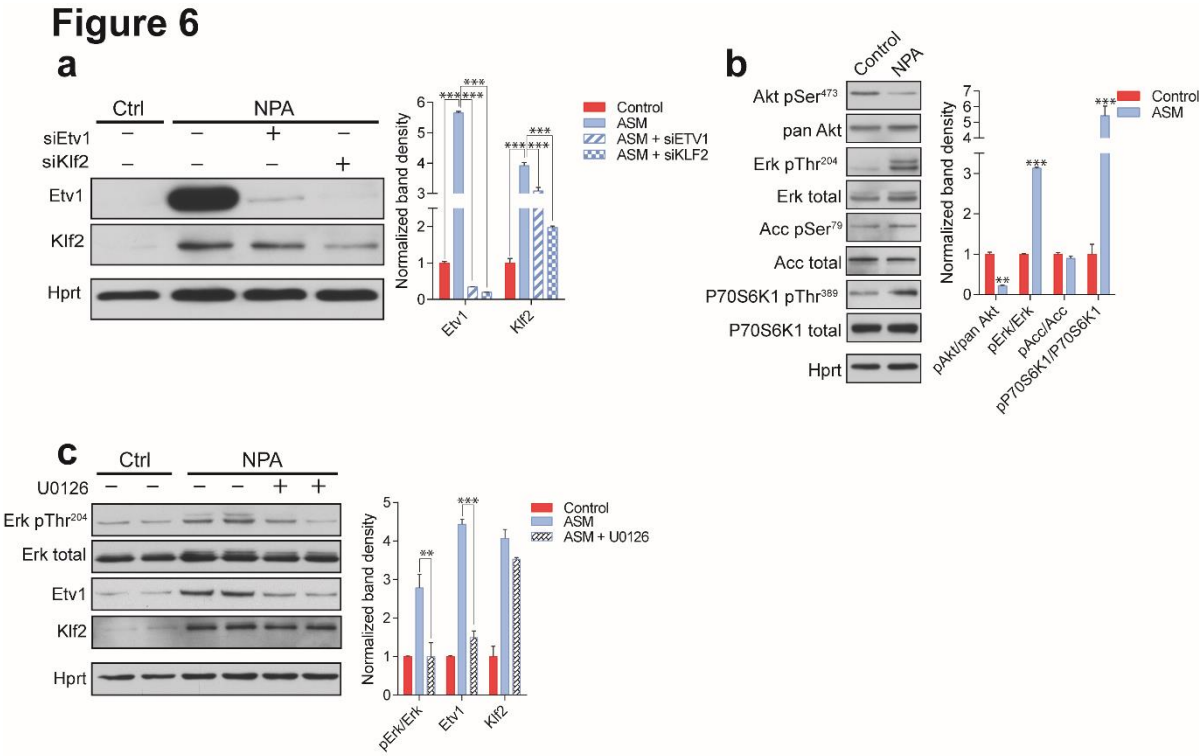

Figure 6. ETV1 up-regulation is dependent on KLF2 and ERK. (a) Silencing of KLF2 in ASM-deficient fibroblasts results in reduced levels of ETV1, shown by a representative (out of three independent experiments) western blot of whole cell extracts, with quantification of band densities (average±stdev) in adjacent plot. ANOVA p-values ***p<0.001 *****p<0.00001. **(b)** ASM-deficient fibroblasts show increased ERK and mTORC1 activities, reduced AKT activity and unchanged AMPK activity, as shown by a representative (out of three independent) western blot of whole cell extracts with band density quantification presented in the adjacent plot. T-test p-values **p<0.01 ***p<0.001 **(c)** ERK inhibition by treatment with U0126 (20μM, 16h) in NP fibroblasts results in reduced ETV1 levels but does not affect KLF2, as shown by a representative western blot, with band density quantification in the adjacent plot. T-test p-values **p<0.01 ***p<0.001

S1PR1 signaling dynamically regulates KLF2 and mitochondrial biogenesis and function

Next, we sought to identify the mechanism leading to KLF2 up-regulation. Since one of the consequences of lysosomal malfunction is the stalling of the autophagy pathway, we tested if KLF2 could be induced by perturbations in autophagy, such as inhibition of autophagosome formation (Atg5 silencing) or inhibition of the fusion of autophagosomes to lysosomes (syntaxin 17 silencing). However, no effect was observed in KLF2 (data not shown).

KLF2 is known to be negatively regulated by Akt signaling (Skon et al., 2013), which is down in ASM-deficient fibroblasts (Figure 6B). Interestingly, one of the genes induced by KLF2 is the sphingosine-1-phosphate receptor 1 (S1PR1) (Skon et al., 2013), which we find up-regulated at transcript level in ASM-deficient fibroblasts (Supplementary Figure S11). S1PR1 and KLF2 are part of a signaling network in which the activity of the receptor represses its own expression by activating Akt, which then phosphorylates KLF2 and marks it for proteasomal degradation (Sinclair et al., 2008; Skon et al., 2013). Interestingly, the S1PR1 receptor has been previously shown to affect mitochondrial function in T cells, but the mechanisms remained unexplored (Mendoza et al., 2017). Furthermore, the levels of sphingosine-1-phosphate (S1P) are decreased in the plasma of NPC patients (Fan et al., 2013), suggesting that signaling elicited by S1P may be down-regulated.

Given the connections between S1PR1, KLF2 and our findings implicating KLF2 in the regulation of mitochondrial-related gene expression, we decided to test if perturbation of the S1PR1 pathway in Niemann-Pick could explain the up-regulation of KLF2 and, accordingly, the expression of mitochondria-related genes. To this end, we treated control fibroblasts with either a selective agonist (Sew2871) or with a selective inhibitor (W146) of S1PR1. Next, we measured the effects on mitochondria. We observed that the activation of S1PR1 by the agonist Sew2871 results in increased transcript levels of mitochondria-related genes (Figure 7A). Reciprocally, inhibition of S1PR1 by W146 leads to decreased transcript levels of these genes. Furthermore, activation of S1PR1 results in increased mitochondrial OCR under

basal and uncoupled conditions (Figure 7C-D), while the inhibition of the receptor results in a robust inhibition of mitochondrial OCR (Figure 7E-F). Finally, we observed that KLF2 responds as expected to S1PR1 activity. When S1PR1 is activated, KLF2 levels decrease (Figure 7G), while inhibition of S1PR1 results in increased KLF2 abundance (Figure 7H). Notably, the protein levels of mitochondrial proteins TFAM, cytochrome oxidase I (mtCOI) and succinate dehydrogenase subunit b (SDHB) are all increased when KLF2 is down-regulated (S1PR1 activation, Figure 7G), and all decreased when KLF2 levels are increased (S1PR1 inhibition, Figure 7H). These results underscore that the S1PR1-KLF2-mitochondrial biogenesis pathway can be dynamically regulated in control fibroblasts. Furthermore, these data suggest that the S1PR1 pathway is down-regulated in ASM-deficient fibroblasts, given the increased levels of KLF2 and the decreased expression of mitochondria-related genes. Interestingly, the expression of sphingosine kinase 1 (SPHK1), which generates S1P that can be exported to the extracellular space, is down-regulated in ASM-deficient fibroblasts (Supplementary Figure S11). Similarly, SPHK2, which generates S1P intracellularly, in mitochondria and endoplasmic reticulum, is also down-regulated in ASM-deficient fibroblasts (Supplementary Figure S11). Altogether, these results suggest that S1P signaling via S1PR1 is profoundly down-regulated in ASM-deficient fibroblasts, and that this event is at the root of the up-regulation of KLF2 and its downstream consequences, particularly ETV1 induction and inhibition of mitochondrial biogenesis.

Figure 7

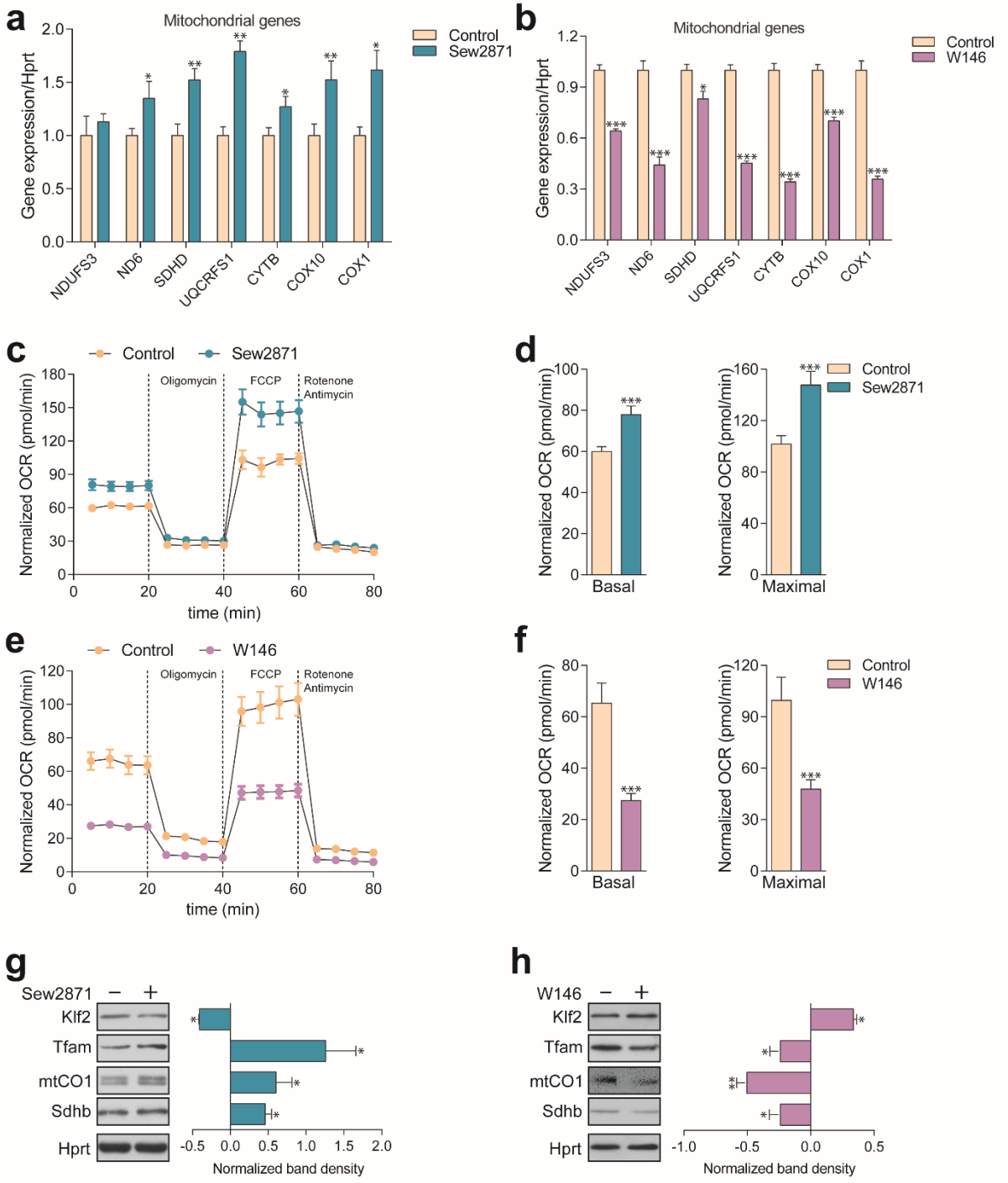

Figure 7. Dynamic regulation of S1PR1 activity impacts mitochondrial biogenesis and function. (a) Transcript levels of mitochondrial-related genes increase upon activation of S1PR1 with the agonist Sew2871 (5μM, 16h; DMSO as vehicle control), as measured by qPCR as described above. Plot shows the average±st.dev. of a representative experiment with three independent replicates, of two independent experiments. **(b)** Transcript levels of mitochondrial-related genes decrease upon inhibition of S1PR1 with the competitive antagonist W146 (10μM, 16h; methanol as vehicle control), as measured by qPCR as described above. Plot shows the average±st.dev. of a representative experiment with three independent replicates, of two independent experiments. **(c-d)** Increased OCR in cells treated with the S1PR1 agonist Sew2871 compared to vehicle control (DMSO), quantified in panel (d). **(e-f)** Decreased OCR in cells treated with the

S1PR1 antagonist W146 compared to vehicle control (methanol), quantified in panel (f). **(g)** Decreased protein levels of KLF2 and increased amounts of mitochondrial proteins TFAM, CO1 and SDHB, in cells treated with S1PR1 agonist Sew2871, assessed by western blots of whole cell extracts, using HPRT as loading control. Plots show the variation compared to vehicle control (DMSO) as average±st.dev. of two independent experiments with two replicates each (the line on zero denotes no change relative to the controls, negative numbers show decrease in fold change treatment/control, positive numbers show increased fold change). T-test p-value *p<0.05 **(h)** Increased protein levels of KLF2 and decreased amounts of mitochondrial proteins TFAM, CO1 and SDHB, in cells treated with S1PR1 antagonist W146, assessed by western blots of whole cell extracts, using HPRT as loading control. Plots show the variation compared to vehicle control (methanol) as average±st.dev. of two independent experiments with two replicates each (the line on zero denotes no change relative to the controls, negative numbers show decrease in fold change treatment/control, positive numbers show increased fold change). T-test p-value *p<0.05 **p<0.01

S11

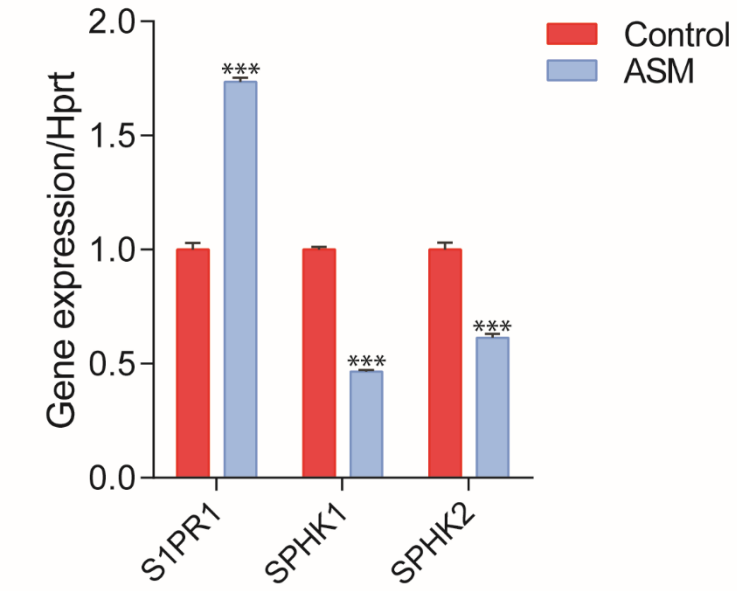

Supplementary Figure 11. Transcript levels of sphingosine-1-phosphate receptor 1 (S1PR1) and sphingosine kinases 1 (SPHK1) and 2 (SPHK2) in ASM-deficient **fibroblasts**. Transcript levels were measured by qPCR, as described above, using three independent biological replicates with two technical replicates for each, and GAPDH (or HPRT, not shown) as control genes. Average±stdev, T-test p-values ***p<0.001

S1PR1 is mislocalized in ASM-deficient cells and unresponsive to activators

Given the apparent down-regulation of S1PR1 signaling in ASM deficiency, we set to test if reactivation of the S1PR1 pathway in ASM-deficient fibroblasts would rescue the expression of mitochondria-related genes as well as mitochondrial function. We treated control and ASM-deficient fibroblasts with the S1PR1 agonist Sew2871, and in agreement with our data shown above, we found an increase in the expression of mitochondria-related genes in control fibroblasts (Figure 8B). However, and surprisingly, the ASM-deficient fibroblasts did not respond to the treatment with the S1PR1 agonist: no change was observed in the transcript levels of mitochondria-related genes (Figure 8B). Similar results were obtained when using S1P instead of the agonist (data not shown). These results suggest that the S1PR1 receptor is absent or inaccessible to extracellular cues, implying that it may be sequestered away from the plasma membrane. The protein levels of S1PR1 are not changed in ASM-deficient fibroblasts (Figure 8C). Therefore, we tested if S1PR1 localization at the plasma membrane was affected in ASM-deficient cells. We used a PE-conjugated antibody against S1PR1 for flow cytometry, in non-permeabilized cells, and determined the amount of plasma membrane labelling in control and ASM-deficient fibroblasts. As negative control, we treated cells with FTY720, which antagonizes S1PR1 signaling by promoting its endocytosis. The treatment with FTY720 reduced the levels of S1PR1 at the plasma membrane, which were robustly decreased in ASM-deficient cells. Thus, the mislocalization of S1PR1 in ASM-deficient cells, and consequent decreased signaling, explain the increase in KLF2 signaling and its downstream consequences.

Figure 8

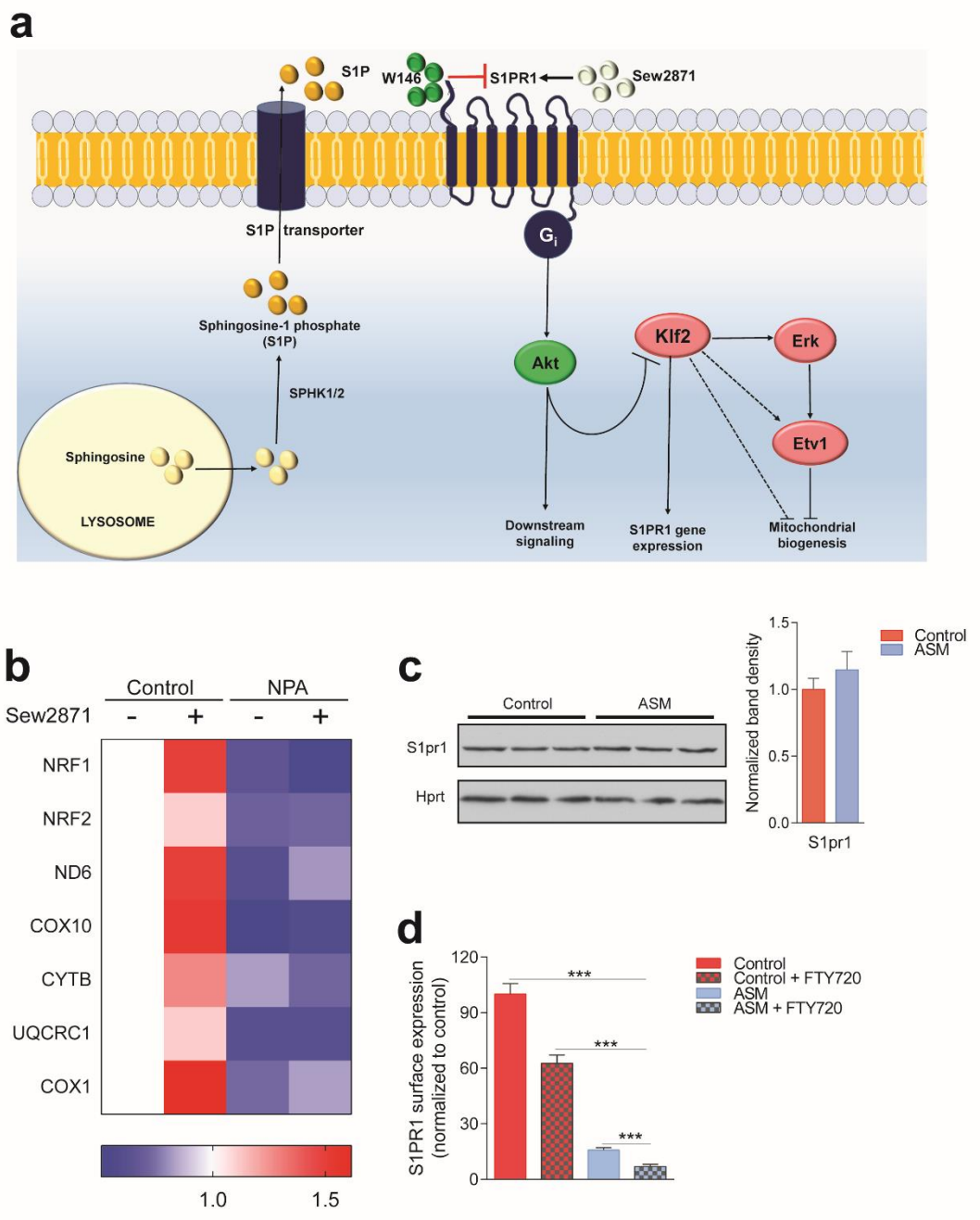

Figure 8. S1PR1 signaling in Niemann-Pick disease
(a) Schematic illustration of sphingosine-1-phospate (S1P) signaling. S1P is generated from sphingosine by the kinases SPHK1 (plasma membrane) and SPHK2 (endoplasmic reticulum and mitochondria), and can be transported out of the cell. Extracellular S1P can activate several receptors (S1PR1-5). Specifically, stimulation of S1PR1 triggers Akt signaling which targets KLF2 for degradation. Expression of S1PR1 is regulated by KLF2, which as shown by our data also activates ETV1. Sew2871 is an agonist of S1PR1, and W146 is an antagonist. **(b)** Treatment of control fibroblasts with S1PR1 agonist Sew2871 (5μM, 16h) results in increased transcript levels of mitochondria-related genes in control fibroblasts, but has no effect on ASM-deficient fibroblasts. The data is presented in a heatmap, in which blue denotes decrease in expression compared to the control cells (white represents no change relative to the control values) and red denotes increase. Note the mostly increased (red) mitochondrial genes in control fibroblasts treated with Sew2871, while blue in ASM fibroblasts regardless of the treatment. **(c)** protein levels of S1PR1 are

not changed in ASM fibroblasts, as measured by western blot using whole cell extracts. Plot shows the quantification of three independent replicates with two technical replicates each. **(d)** staining of S1PR1 present at the plasma membrane, in non-permeabilized cells, measured by flow cytometry. FTY720 triggers the endocytosis if S1PR1 and was used as a negative control for surface staining.

DISCUSSION

This study addresses a novel mechanism by which mitochondria are impaired in lysosomal lipid storage diseases. We show here that the transcription factors KLF2 and ETV1 repress the expression of genes encoding mitochondrial proteins. Both KLF2 and ETV1 are up-regulated in patient cells from Niemann-Pick type C and acid sphingomyelinase deficiency, and their silencing, particularly KLF2, is sufficient to return mitochondrial biogenesis and function to control levels. Decreased signaling through sphingosine-1-phosphate receptor 1 (S1PR1) activates KLF2, which induces the expression of ETV1, culminating in the down-regulation of mitochondrial biogenesis.

The transcriptional regulation of mitochondrial biogenesis is known since the identification of the transcription factor nuclear respiratory factor 1 (NRF1), which induces the expression of many respiratory chain and mtDNA maintenance genes (Scarpulla et al., 2012). Several other transcription factors have been shown to stimulate mitochondrial biogenesis, such as estrogen related receptor α (ERRα) or the oncogene myc (Scarpulla et al., 2012). The role of the co-activator PGC1α (peroxisome proliferation activated receptor gamma, co-activator 1α) has also been shown to promote NRF1- and ERRα-mediated mitochondrial biogenesis (Wu et al., 1999). However, to our knowledge, no transcription factor has previously been shown to repress mitochondrial biogenesis. Thus, the roles of KLF2 and ETV1 as repressors of mitochondrial biogenesis, shown in this manuscript, open a new paradigm on the transcriptional regulation of the mitochondrial biogenesis. Notably, the transcription factor NRF1, which is a known positive regulator of mitochondrial biogenesis and is down-regulated in fibroblasts with acid sphingomyelinase deficiency, is also repressed by KLF2 and ETV1. It therefore seems that KLF2, ETV1 and NRF1 may form a transcriptional regulatory network that dynamically regulates mitochondrial biogenesis, with accelerator (NRF1) and brakes (KLF2 and ETV1). The transcriptional network between KLF2, ETV1 and NRF1, as well as the involvement of other transcription factors such as ERRα, myc, or co-activators such as PGC1α, warrants further research. Interestingly, another Krüppel-like factor, KLF4, was

recently shown to promote mitochondrial biogenesis in the heart (Liao et al., 2015), implying that the repressive behavior of KLF2 is a specificity of this transcription factor and not a characteristic transversal to the whole Krüppel-like factor family.

It is particularly interesting that a transcriptional network repressing mitochondrial biogenesis appears robustly active in lysosomal diseases. The role of lysosomes in cellular function has been subject of increasing attention, both regarding its physiological roles as a signaling platform as well as the pathological consequences of lysosomal defects in lysosomal storage diseases (Settembre et al., 2008; Ballabio and Gieselmann, 2009; Perera and Zoncu, 2016; Platt et al., 2012). Numerous studies describe the impact of lysosomal defects on the function of other organelles, particularly mitochondria, in several lysosomal storage diseases (Diogo et al., 2017; Plotegher and Duchen, 2017; Raimundo et al., 2016; Torres et al., 2017). Mitochondria are usually impaired in cells and tissues with primary lysosomal defects, with decreased oxygen consumption and increased production of superoxide and other reactive oxygen species (Jolly et al., 2002; Plotegher and Duchen, 2017). However, this is usually attributed to a decrease in autophagy (and mitophagy), with the consequent accumulation of damaged mitochondria in the cytoplasm. Our data in cellular and mouse models of Niemann-Pick-C disease and acid sphingomyelinase deficiency shows, however, that in addition to defective autophagy there is a signaling mechanism based on the induction of two transcription factors, KLF2 and ETV1, which repress mitochondrial biogenesis. This may represent a signaling circuit in which the cells with lysosomal defects repress the generation of an organelle whose degradation requires lysosomal function.

Interestingly, the up-regulation of KLF2 in ASM-deficient cells seems to be a consequence of impaired sphingosine-1-phosphate (S1P) signaling through S1P receptor 1 (S1PR1). This receptor had previously been implicated in the regulation of mitochondrial function in T cells, but the mechanism remained unclear (Mendoza et al., 2017). We show in this study that S1PR1 is a bona fide bi-directional regulator of mitochondrial function via the effect of KLF2 and ETV1 on mitochondrial biogenesis. Indeed, both the activation and the inhibition of

S1PR1 impacted the expression of genes encoding mitochondrial proteins in control cells. Interestingly, the acid sphingomyelinase-deficient fibroblasts were non-responsive to agonists of S1PR1, which suggests that the receptor may be sequestered away from the plasma membrane in the patient cells. In support of this hypothesis, the amount of S1PR1 in the plasma membrane of the ASM-deficient cells is negligible, while the total protein levels of S1PR1 are similar to control cells. This result implies a mistargeting of S1PR1 in acid sphingomyelinase deficiency and Niemann-Pick disease, which is akin to other proteins aberrantly mislocalized away from the plasma membrane in these diseases, such as Met receptor tyrosine kinase or K-Ras (Zhu et al., 2016; Cho et al., 2015).

The accumulation of lipids such as sphingomyelin and cholesterol in the lysosomes in Niemann-Pick type C and acid sphingomyelinase deficiency is likely to result in deficiency of those lipids in other cellular locations. Thus, one conceivable cellular adaptation would be shutting down the mitochondrial respiratory chain and citrate cycle, which would allow to shunt citrate to the cytoplasm, where it can be converted by acetyl-CoA lyase to acetyl-CoA and used for lipid synthesis (Bauer et al., 2005; Wellen et al., 2009).

The interplay between mitochondria and lysosomes is a relatively novel concept that only now starts being grasped (Diogo et al., 2017; Raimundo et al., 2016). Our study contributes to the understanding of how mitochondria and lysosomes are interdependent. By identifying a molecular mechanism involving a transcriptional network, we highlight that the communication between these two organelles goes beyond metabolic cues, and involves complex cellular signaling. This is akin to what is observed in mitochondrial malfunction, which also impacts the transcriptional programs of lysosomal biogenesis (Fernandez-Mosquera et al., 2017; Nezich et al., 2015).

The contribution of the signaling pathways mediating communication between mitochondria and lysosomes for pathology certainly warrants further exploration, not just in mitochondrial and lysosomal diseases but also in the context of neurodegenerative diseases that arise from defects of either of these organelles.

MATERIAL AND METHODS

Drugs and cellular treatments

The following drugs were used for cellular treatments: 50µM Chloroquine (Sigma, C6628), 1µM Oligomycin (Sigma, O4876), 2µM Carbonyl cyanide 3-fluorophenylhydrazone (FCCP) (Sigma, C2920), 1µM Rotenone (Sigma, R8875), 1µM Antimycin (Sigma, A8674), 40µM Desipramine (Biotrend, BG0162), 5µM Sew2871 (Cayman, 10006440), 20µM U0126 (Millipore, 662005), 10µM U18666A (Cayman, 10009085), 10µM W146 (Sigma-Aldrich, W1020) and 2µM FTY720 (Selleckchem, S5002).

Cell culture and transient transfections

Control and Niemann-Pick patient fibroblasts were grown in DMEM high glucose medium (Gibco, 11965) supplemented with 10% fetal bovine serum and 1% Penicillin/Streptomycin at 37°C and 5% CO2, in a humidified incubator, unless otherwise stated. Patient fibroblasts retained about 5% of the control activity of acid sphingomyelinase, and were collected and maintained according to the ethical guidelines of the UMG. Control and patient fibroblasts were transfected with siRNAs for ETV1 or KLF2 using electroporation (Amaxa kit, Lonza, V4XP-1024) or with scrambled control siRNA following manufacturer's protocol. Additional control, human, adult primary fibroblasts were obtained ATCC (PCS-201-012). NPC1 patient cells were obtained from Coriell Institute for Medical Research (GM18398). The use of human cells for these studies was approved by the Ethical Commision of the Universitätsmedizin Göttingen.

XF medium

XF assay medium (Seahorse Bioscience, 100965-000) was supplemented with sodium pyruvate, glutamax and glucose following manufacturer's recipe and the pH of medium was adjusted to 7.4.

Oxygen consumption rate measurements

OCR was measured in fibroblasts using the XF96 Extracellular Flux analyzer (Seahorse Bioscience) as described (53). Briefly, cells were seeded at 20000 cells per well in XF96 cell culture multi-well plates in DMEM medium and incubated for 24 hours in the growth conditions stated for all cell cultures. XF96 cartridges were incubated overnight in XF calibrant at 370C in a non-CO2 incubator. Prior to OCR measurements, the growth medium of cells was exchanged with XF medium and incubated at 370C in a non-CO2 incubator for 1hour. Inhibitors were diluted to appropriate concentrations in XF medium and loaded into corresponding microwells in the XF96cartridge plate. Following equilibration of sensor cartridges, XF96 cell culture plate was loaded into the XF96 Extracellular Flux analyzer at 370C and OCR was measured after cycles of mixing and acquiring data (basal) or inhibitor injection, mixing and data acquisition.

Western Blotting

Whole cell extracts of cultured fibroblast were prepared in 1.5% n-dodecylmaltoside (Roth, CN26.2) in PBS supplemented with protease and phosphatase inhibitor cocktail (Thermoscientific, 78442) as described (Raimundo et al, 2009). Protein concentrations of whole cell extracts were determined using a Bradford assay (Bio-Rad, 500-0006). 50µg of sample proteins per well were subjected to Sodium dodecyl sulfate -polyacrylamide gel electrophoresis (SDS-PAGE) and transferred to polyvinylidene fluoride (PVDF) membranes (Amersham, Life Technologies). After blocking in 5% Milk in TBS tween, membranes were

immunoblotted with the following antibodies: SQSTM1 (Abcam, ab110252), HPRT (Abcam, ab10479), KLF2 (Abcam, ab203591), ETV1 (Abcam, ab184120), LC3B (Cell signaling, 3868), Pan Akt (Cell signaling, 4691), Phospho Akt (Cell signaling, 4060), Total Erk1/2(Cell signaling, 4695), Phospho Erk1/2 (Cell signaling, 4376), TFAM (Abcam, ab138351), P70S6K1 (Cell signaling, 2708) phospho P70S6K1 (9234), ACC (Cell signaling, 3676), phospho ACC (Cell signaling, 3661), Nrf1 (Abcam, ab175932), Nrf2 (Proteintech, 21542-1-AP) and Uqcrc1 (Abcam, ab110252), Tfeb (Bethyl, A303-672A), Ndufs3 (Invitrogen, 459130), Sdhb, mtCO1 OXPHOS cocktail (Abcam, ab110413) and S1PR1 (Abcam, ab125074).. Band densitometric quantifications were determined using ImageJ software 1.48v.

Quantitative RT-PCR

RNA extraction and purification from fibroblasts were performed using Crystal RNA mini Kit (Biolab, 31-01-404). RNA extraction from mouse liver was performed using Trizol as described (Fernandez-Mosquera et al., 2017) followed by purification using Crystal RNA mini kit (Biolab, 31-01-404). RNA concentration and quality were determined using Nanodrop (PeqLab) and cDNA was synthesized with iScript cDNA synthesis kit (Bio-Rad, 178-8991) following manufacturer's protocol. Each 8µl q-PCR was made of 4µl diluted cDNA, 0.2µl of each primer (from 25µM stock) and 3.6µl of iTaq Universal Sybr Green Supermix (Bio-Rad, 172-5124) and ran on the QuantStudio 6 Flex Real-Time PCR system (Applied Biosystems).

Flow Cytometry

Measurement of mitochondrial superoxide levels using MitoSOX Red Mitochondrial superoxide indicator (Molecular Probes, M36008) was performed by flow cytometry according to the manufacturer's instructions. For S1PR1 plasma membrane localization, $1x10^6$ control and ASM deficient fibroblasts treated with or without 2µM FTY720 were labelled in suspension with 10µL of PE-conjugated S1PR1 antibody (R and D systems,

FAB2016P) for 1hour, washed twice in isotonic PBS supplemented with 1% BSA, resuspended in 200-400uL of buffer and subjected to flow cytometry analyses for the surface expression of S1PR1.

Statistical Analysis

The results obtained from at least three independent replicates were presented as mean ± SD unless otherwise indicated. P-values were determined using Student´s t test for two group comparisons or ANOVA for multi-group comparisons. *p<0.05 **p<0.01 ***p<0.001.

Dataset selection

In order to identify transcriptional signatures mediating interactions between organelles in Niemann-Pick pathology, we mined for microarray data involving Niemann-Pick mouse models from the Gene Expression Omnibus (http://www.ncbi.nlm.nih.gov/geo). Criteria for dataset selection included datasets with multiple replicates from several tissues. The dataset selected was GSE39621, which includes samples of brain, liver and spleen of mice before and after 6 weeks of age, when the symptoms of the disease start manifesting. Given that the spleen may contain immune cells in addition to splenocytes, and likely to have many more of non-splenocytes in the disease case, since spleen enlargement is a hallmark of the disease, we considered that the control and NPC1-/- were not directly comparable and thus used only the data relative to brain and liver.

Organelle-specific gene lists

We obtained organelle proteomes from up-to-date and comprehensive databases for mitochondrial (and respiratory chain subunits), lysosomal, peroxisomal, endoplasmic reticulum and Golgi proteomes (Table I). These protein IDs were converted to NCBI gene

symbols, which were then used to identify the corresponding probeset names for different microarray matrices.

Microarray data analysis

We obtained mouse NPC1 wildtype, NPC1+/- and NPC1-/- in asymptomatic (less than 6 weeks old) and symptomatic (more than 6 weeks old) brain, liver and spleen from the GEO database (Alam et al., 2012). The controls for the NPC1 dataset are the wt mice in the brain but the heterozygous mice in the other tissues. We used the software GeneSpring (Agilent Technologies, Santa Clara, CA) to normalize the datasets by robust multi-array averaging (RMA) to normalize datasets (Raimundo et al., 2009). The datasets for all tissues originating from the same knock-out mouse and corresponding controls were normalized together. After normalization, we determined which transcripts had significantly different expression between NPC1-/- and controls for each individual tissue, using ANOVA. We also calculated the fold change from probe expression values between lysosomal disease and control mice for each tissue. The statistical filter was set at p-value<0.05, and the transcripts that pass the filter for each tissue represent the corresponding transcriptional signature.

To calculate the average expression of organelle-specific gene lists, we normalized each transcript to the average of the control samples, and calculated the average of the expression levels of all genes in each organelle-specific gene list. To determine if the difference observed between NPC-/- and controls was significant, we calculated the t-test p-value (unpaired, unequal variance) for the whole gene set using Microsoft Excel. Given that the lists have hundreds of genes, we performed a Bonferroni post-hoc correction. The adjusted p-values<0,05 were considered significant.

Pathway analysis and identification of transcriptional regulators

We employed a multi-dimensional strategy aimed at the identification of signaling pathways, as described (Raimundo et al., 2012; Raimundo et al., 2009; Schroeder et al., 2013; West et al., 2015). The transcriptional lists were imported to the software Ingenuity Pathway Analysis (IPA) (http://www.ingenuity.com), which then determines which pathways and transcriptional regulators are statistically enriched, using Fisher's exact test. The statistical threshold was set at $p<0.01$.

Promoter analysis

To perform promoter analysis on the respiratory chain genes, we imported the respiratory chain gene list to the software Genomatix Suite (www.genomatix.de). Then we set a pipeline within the software suite, by first defining the promoters of the respiratory chain genes and then determining which transcription factors (TF) had binding sites on them. To locate the promoters, we use the Genomatix tool Gene2Promoter, and defined the promoter region from 500 base pairs upstream (-500) the transcription start site (TSS) until 100 base pairs downstream the TSS (+100). Given that some genes may have more than one promoter due to alternative splicing, we selected only the promoters that drive the expression of the transcript leading to the protein that functions as a respiratory chain subunit. The promoter sequences were then used to determine cis-elements and identify the corresponding TF, limiting the search to those TF that had at least a binding site in at least 85% of the promoters. The software provides a statistical assessment of the enrichment of the binding sites for each TF family in the promoters under analysis. We set a threshold of $p<0.05$ for the Fisher exact test p-value for each TF family enrichment. Then, we determine, for each significantly enriched family, which individual TF are included, and select as relevant TF those that have a binding site in at least 50% of the promoters under analysis.

Accession numbers

The publicly-available dataset used in this study is GSE39621 for Niemann Pick's disease mouse model (NPC1-/-) (Alam et al., 2012).

Measurement of lysosomal proteolytic capacity

Lysosomal proteolytic capacity was measured using the DQ Red BSA Dye (Molecular Probes, D-12051) following manufacturer's protocol. 1mg of dye is resuspended in 1mL of PBS and 100ul of the resuspended dye is added to 10ml of warm DMEM medium. Previously plated cells in a transparent 96 well-plate are loaded with 100ul per well each of the dye containing medium and incubated at 37°C for 1 hour. Cells are then washed twice with warm PBS and the medium is replaced with 100 µL/well of warm EBSS medium. The kinetics of DQ Red BSA digestion are recorded at respective excitation and emission maxima of 590nm and 620nm in a multi-plate reader over a 4h period.

ACKNOWLEDGEMENTS

ERC Starting Grant 337327 and AMDA Research Grant (NR); Deutsche Forschungsgemeinschaft Emmy-Noether Award and Schram Stiftung Grant (IM); Deutsche Forschungsgemeinschaft SFB1190 (NR and IM).

We thank Dr. Ralf Janknecht for the ETV1 constructs.

CONFLICT OF INTEREST STATEMENT

The authors have no conflict of interest.

TABLES

Table I. Sources of organelle-specific proteomes.

Dataset	Number of genes	Reference (source)
Mitochondria	1049	(Pagliarini et al., 2008)
Respiratory chain subunits	108	(Pagliarini et al., 2008)
Lysosomes	435	(Brozzi et al., 2013)
Peroxisomes	254	(Wiese et al., 2007)
Endoplasmic reticulum	297	(Gilchrist et al., 2006)
Golgi (COP I) Vesicles	86	(Gilchrist et al., 2006)

Table II. Transcription factors with statistically enriched cis-elements in the promoters of genes encoding for subunits of mitochondrial respiratory chain.

Transcription factor family	p-value (Fisher exact test)	Transcription factors
SP1	1.52E-09	SP1, SP4
E2F	2.79E-08	E2F1, E2F2, E2F3, E2F4
KLF	0.000265	KLF2, KLF6, KLF7, KLF15
ETS	0.000796	ELK1, SPI1, ETV1

REFERENCES

Alam, M.S., Getz, M., Safeukui, I., Yi, S., Tamez, P., Shin, J., Velazquez, P., and Haldar, K. (2012). Genomic expression analyses reveal lysosomal, innate immunity proteins, as disease correlates in murine models of a lysosomal storage disorder. PLoS One *7*, e48273.

Baena, E., Shao, Z., Linn, D.E., Glass, K., Hamblen, M.J., Fujiwara, Y., Kim, J., Nguyen, M., Zhang, X., Godinho, F.J.*, et al.* (2013). ETV1 directs androgen metabolism and confers aggressive prostate cancer in targeted mice and patients. Genes Dev *27*, 683-698.

Ballabio, A. (2016). The awesome lysosome. EMBO Mol Med *8*, 73-76.

Ballabio, A., and Gieselmann, V. (2009). Lysosomal disorders: from storage to cellular damage. Biochim Biophys Acta *1793*, 684-696.

Bauer, D.E., Hatzivassiliou, G., Zhao, F., Andreadis, C., and Thompson, C.B. (2005). ATP citrate lyase is an important component of cell growth and transformation. Oncogene *24*, 6314-6322.

Corcelle-Termeau E, Vindeløv SD, Hämälistö S, Mograbi B, Keldsbo A, Bräsen JH, Favaro E, Adam D, Szyniarowski P, Hofman P, Krautwald S, Farkas T, Petersen NH, Rohde M, Linkermann A, Jäättelä M (2016). Excess sphingomyelin disturbs ATG9A trafficking and autophagosome closure. Autophagy *12*, 833-849

Cotney, J., McKay, S.E., and Shadel, G.S. (2009). Elucidation of separate, but collaborative functions of the rRNA methyltransferase-related human mitochondrial transcription factors B1 and B2 in mitochondrial biogenesis reveals new insight into maternally inherited deafness. Hum Mol Genet *18*, 2670-2682.

Das, H., Kumar, A., Lin, Z., Patino, W.D., Hwang, P.M., Feinberg, M.W., Majumder, P.K., and Jain, M.K. (2006). Kruppel-like factor 2 (KLF2) regulates proinflammatory activation of monocytes. Proc Natl Acad Sci U S A *103*, 6653-6658.

Diogo, C.V., Yambire, K.F., Fernandez Mosquera, L., Branco, F.T., and Raimundo, N. (2017). Mitochondrial adventures at the organelle society. Biochem Biophys Res Commun.

Dugas, J.C., Tai, Y.C., Speed, T.P., Ngai, J., and Barres, B.A. (2006). Functional genomic analysis of oligodendrocyte differentiation. J Neurosci *26*, 10967-10983.

Evans, M.J., and Scarpulla, R.C. (1989). Interaction of nuclear factors with multiple sites in the somatic cytochrome c promoter. Characterization of upstream NRF-1, ATF, and intron Sp1 recognition sequences. J Biol Chem *264*, 14361-14368.

Evans, M.J., and Scarpulla, R.C. (1990). NRF-1: a trans-activator of nuclear-encoded respiratory genes in animal cells. Genes Dev *4*, 1023-1034.

Fabre, S., Lang, V., Harriague, J., Jobart, A., Unterman, T.G., Trautmann, A., and Bismuth, G. (2005). Stable activation of phosphatidylinositol 3-kinase in the T cell immunological synapse stimulates Akt signaling to FoxO1 nuclear exclusion and cell growth control. Journal of immunology (Baltimore, Md : 1950) *174*, 4161-4171.

Fan M, Sidhu R, Fujiwara H, Tortelli B, Zhang J, Davidson C, Walkley SU, Bagel JH, Vite C, Yanjanin NM, Porter FD, Schaffer JE, Ory DS (2013). Identification of Niemann-Pick C1 disease biomarkers through sphingolipid profiling. J Lipid Res. 54: 2800-2814

Feng, R., Desbordes, S.C., Xie, H., Tillo, E.S., Pixley, F., Stanley, E.R., and Graf, T. (2008). PU.1 and C/EBPalpha/beta convert fibroblasts into macrophage-like cells. Proc Natl Acad Sci U S A *105*, 6057-6062.

Fernandez-Mosquera, L., Diogo, C.V., Yambire, K.F., Santos, G.L., Luna Sanchez, M., Benit, P., Rustin, P., Lopez, L.C., Milosevic, I., and Raimundo, N. (2017). Acute and chronic mitochondrial respiratory chain deficiency differentially regulate lysosomal biogenesis. Sci Rep *7*, 45076.

Gleyzer, N., Vercauteren, K., and Scarpulla, R.C. (2005). Control of mitochondrial transcription specificity factors (TFB1M and TFB2M) by nuclear respiratory factors (NRF-1 and NRF-2) and PGC-1 family coactivators. Mol Cell Biol *25*, 1354-1366.

Herzog, B., Cardenas, J., Hall, R.K., Villena, J.A., Budge, P.J., Giguere, V., Granner, D.K., and Kralli, A. (2006). Estrogen-related receptor alpha is a repressor of phosphoenolpyruvate carboxykinase gene transcription. J Biol Chem *281*, 99-106.

Hollenhorst, P.C., Shah, A.A., Hopkins, C., and Graves, B.J. (2007). Genome-wide analyses reveal properties of redundant and specific promoter occupancy within the ETS gene family. Genes Dev *21*, 1882-1894.

Horinouchi K, Erlich S, Perl DP, Ferlinz K, Bisgaier CL, Sandhoff K, Desnick RJ, Stewart CL, Schuchman EH (1995). Acid sphingomyelinase deficient mice: a model of types A and B Niemann-Pick disease. Nat Genet. 10:288-293.

Janknecht, R. (1996). Analysis of the ERK-stimulated ETS transcription factor ER81. Mol Cell Biol *16*, 1550-1556.

Jolly, R.D., Brown, S., Das, A.M., and Walkley, S.U. (2002). Mitochondrial dysfunction in the neuronal ceroid-lipofuscinoses (Batten disease). Neurochem Int *40*, 565-571.

Kasahara, A., and Scorrano, L. (2014). Mitochondria: from cell death executioners to regulators of cell differentiation. Trends Cell Biol *24*, 761-770.

Kennedy, B.E., Madreiter, C.T., Vishnu, N., Malli, R., Graier, W.F., and Karten, B. (2014). Adaptations of energy metabolism associated with increased levels of mitochondrial cholesterol in Niemann-Pick type C1-deficient cells. J Biol Chem *289*, 16278-16289.

Kerdiles, Y.M., Beisner, D.R., Tinoco, R., Dejean, A.S., Castrillon, D.H., DePinho, R.A., and Hedrick, S.M. (2009). Foxo1 links homing and survival of naive T cells by regulating L-selectin, CCR7 and interleukin 7 receptor. Nature immunology *10*, 176-184.

Kirkegaard, T., Roth, A.G., Petersen, N.H., Mahalka, A.K., Olsen, O.D., Moilanen, I., Zylicz, A., Knudsen, J., Sandhoff, K., Arenz, C*., et al.* (2010). Hsp70 stabilizes lysosomes and reverts Niemann-Pick disease-associated lysosomal pathology. Nature *463*, 549-553.

Leventhal, A.R., Chen, W., Tall, A.R., and Tabas, I. (2001). Acid sphingomyelinase-deficient macrophages have defective cholesterol trafficking and efflux. J Biol Chem *276*, 44976-44983.

Li, F., Wang, Y., Zeller, K.I., Potter, J.J., Wonsey, D.R., O'Donnell, K.A., Kim, J.W., Yustein, J.T., Lee, L.A., and Dang, C.V. (2005). Myc stimulates nuclearly encoded mitochondrial genes and mitochondrial biogenesis. Mol Cell Biol *25*, 6225-6234.

Liao, X., Zhang, R., Lu, Y., Prosdocimo, D.A., Sangwung, P., Zhang, L., Zhou, G., Anand, P., Lai, L., Leone, T.C*., et al.* (2015). Kruppel-like factor 4 is critical for transcriptional control of cardiac mitochondrial homeostasis. J Clin Invest *125*, 3461-3476.

Lim, C.Y., and Zoncu, R. (2016). The lysosome as a command-and-control center for cellular metabolism. J Cell Biol *214*, 653-664.

Lim, J.A., Li, L., Kakhlon, O., Myerowitz, R., and Raben, N. (2015). Defects in calcium homeostasis and mitochondria can be reversed in Pompe disease. Autophagy *11*, 385-402.

Lloyd-Evans E, Morgan AJ, He X, Smith DA, Elliot-Smith E, Sillence DJ, Churchill GC, Schuchman EH, Galione A, Platt FM (2008). Niemann-Pick disease type C1 is a sphingosine storage disease that causes deregulation of lysosomal calcium. Nat Med. *14*: 1247-1255

Loftus, S.K., Morris, J.A., Carstea, E.D., Gu, J.Z., Cummings, C., Brown, A., Ellison, J., Ohno, K., Rosenfeld, M.A., Tagle, D.A*., et al.* (1997). Murine model of Niemann-Pick C disease: mutation in a cholesterol homeostasis gene. Science *277*, 232-235.

Mendoza, A., Fang, V., Chen, C., Serasinghe, M., Verma, A., Muller, J., Chaluvadi, V.S., Dustin, M.L., Hla, T., Elemento, O*., et al.* (2017). Lymphatic endothelial S1P promotes mitochondrial function and survival in naive T cells. Nature *546*, 158-161.

Nezich, C.L., Wang, C., Fogel, A.I., and Youle, R.J. (2015). MiT/TFE transcription factors are activated during mitophagy downstream of Parkin and Atg5. J Cell Biol *210*, 435-450.

Osellame, L.D., Rahim, A.A., Hargreaves, I.P., Gegg, M.E., Richard-Londt, A., Brandner, S., Waddington, S.N., Schapira, A.H., and Duchen, M.R. (2013). Mitochondria and quality control defects in a mouse model of Gaucher disease--links to Parkinson's disease. Cell Metab *17*, 941-953.

Pagliarini, D.J., Calvo, S.E., Chang, B., Sheth, S.A., Vafai, S.B., Ong, S.E., Walford, G.A., Sugiana, C., Boneh, A., Chen, W.K., *et al.* (2008). A mitochondrial protein compendium elucidates complex I disease biology. Cell *134*, 112-123.

Pagliarini, D.J., and Rutter, J. (2013). Hallmarks of a new era in mitochondrial biochemistry. Genes Dev *27*, 2615-2627.

Parenti, G., Andria, G., and Ballabio, A. (2015). Lysosomal storage diseases: from pathophysiology to therapy. Annual review of medicine *66*, 471-486.

Patterson, M.C., and Walkley, S.U. (2017). Niemann-Pick disease, type C and Roscoe Brady. Mol Genet Metab *120*, 34-37.

Pentchev PG, Boothe AD, Kruth HS, Weintroub H, Stivers J, Brady RO (1984). A genetic storage disorder in BALB/C mice with a metabolic block in esterification of exogenous cholesterol. J Biol Chem. *259*: 5784-5791

Perera, R.M., and Zoncu, R. (2016). The Lysosome as a Regulatory Hub. Annu Rev Cell Dev Biol *32*, 223-253.

Pickles, S., Vigie, P., and Youle, R.J. (2018). Mitophagy and Quality Control Mechanisms in Mitochondrial Maintenance. Curr Biol *28*, R170-R185.

Platt, F.M. (2014). Sphingolipid lysosomal storage disorders. Nature *510*, 68-75.

Platt, F.M., Boland, B., and van der Spoel, A.C. (2012). The cell biology of disease: lysosomal storage disorders: the cellular impact of lysosomal dysfunction. J Cell Biol *199*, 723-734.

Plotegher, N., and Duchen, M.R. (2017). Mitochondrial Dysfunction and Neurodegeneration in Lysosomal Storage Disorders. Trends Mol Med *23*, 116-134.

Poon, G.M. (2012). DNA binding regulates the self-association of the ETS domain of PU.1 in a sequence-dependent manner. Biochemistry *51*, 4096-4107.

Praggastis M, Tortelli B, Zhang J, Fujiwara H, Sidhu R, Chacko A, Chen Z, Chung C, Lieberman AP, Sikora J, Davidson C, Walkley SU, Pipalia NH, Maxfield FR, Schaffer JE, Ory DS (2015). A murine Niemann-Pick C1 I1061T knock-in model recapitulates the pathological features of the most prevalent human disease allele. J Neurosci. 35: 8091-8106

Raimundo, N. (2014). Mitochondrial pathology: stress signals from the energy factory. Trends Mol Med *20*, 282-292.

Raimundo, N., Fernandez-Mosquera, L., Yambire, K.F., and Diogo, C.V. (2016). Mechanisms of communication between mitochondria and lysosomes. Int J Biochem Cell Biol *79*, 345-349.

Raimundo, N., Song, L., Shutt, T.E., McKay, S.E., Cotney, J., Guan, M.X., Gilliland, T.C., Hohuan, D., Santos-Sacchi, J., and Shadel, G.S. (2012). Mitochondrial Stress Engages E2F1 Apoptotic Signaling to Cause Deafness. Cell *148*, 716-726.

Raimundo, N., Vanharanta, S., Aaltonen, L.A., Hovatta, I., and Suomalainen, A. (2009). Downregulation of SRF-FOS-JUNB pathway in fumarate hydratase deficiency and in uterine leiomyomas. Oncogene *28*, 1261-1273.

Scarpulla, R.C., Vega, R.B., and Kelly, D.P. (2012). Transcriptional integration of mitochondrial biogenesis. Trends Endocrinol Metab *23*, 459-466.

Schroeder, E.A., Raimundo, N., and Shadel, G.S. (2013). Epigenetic silencing mediates mitochondria stress-induced longevity. Cell Metab *17*, 954-964.

Schuchman, E.H., and Wasserstein, M.P. (2016). Types A and B Niemann-Pick Disease. Pediatric endocrinology reviews : PER *13 Suppl 1*, 674-681.

Settembre C, Fraldi A, Jahreiss L, Spampanato C, Venturi C, Medina D, de Pablo R, Tacchetti C, Rubinsztein DC, Ballabio A. (2008). A block of autophagy in lysosomal storage disorders. Hum Mol Genet. 17:119-129

Settembre, C., Fraldi, A., Medina, D.L., and Ballabio, A. (2013). Signals from the lysosome: a control centre for cellular clearance and energy metabolism. Nat Rev Mol Cell Biol *14*, 283-296.

Sinclair LV, Finlay D, Feijoo C, Cornish GH, Gray A, Ager A, Okkenhaug K, Hagenbeek TJ, Spits H, Cantrell DA. (2008). Phosphatidylinositol-3-OH kinase and nutrient-sensing mTOR pathways control T lymphocyte trafficking. Nat Immunol. *9*, 513-21.

Skon, C.N., Lee, J.Y., Anderson, K.G., Masopust, D., Hogquist, K.A., and Jameson, S.C. (2013). Transcriptional downregulation of S1pr1 is required for the establishment of resident memory CD8+ T cells. Nature immunology *14*, 1285-1293.

Speak, A.O., Te Vruchte, D., Davis, L.C., Morgan, A.J., Smith, D.A., Yanjanin, N.M., Simmons, L., Hartung, R., Runz, H., Mengel, E.*, et al.* (2014). Altered distribution and function of natural killer cells in murine and human Niemann-Pick disease type C1. Blood *123*, 51-60.

Suzuki, T., Nakano-Ikegaya, M., Yabukami-Okuda, H., de Hoon, M., Severin, J., Saga-Hatano, S., Shin, J.W., Kubosaki, A., Simon, C., Hasegawa, Y.*, et al.* (2012). Reconstruction of monocyte transcriptional regulatory network accompanies monocytic functions in human fibroblasts. PLoS One *7*, e33474.

Torres, S., Balboa, E., Zanlungo, S., Enrich, C., Garcia-Ruiz, C., and Fernandez-Checa, J.C. (2017). Lysosomal and Mitochondrial Liaisons in Niemann-Pick Disease. Frontiers in physiology *8*, 982.

Vanier, M.T. (1983). Biochemical studies in Niemann-Pick disease. I. Major sphingolipids of liver and spleen. Biochim Biophys Acta *750*, 178-184.

Virbasius, J.V., and Scarpulla, R.C. (1994). Activation of the human mitochondrial transcription factor A gene by nuclear respiratory factors: a potential regulatory link between nuclear and mitochondrial gene expression in organelle biogenesis. Proc Natl Acad Sci U S A *91*, 1309-1313.

Wellen, K.E., Hatzivassiliou, G., Sachdeva, U.M., Bui, T.V., Cross, J.R., and Thompson, C.B. (2009). ATP-citrate lyase links cellular metabolism to histone acetylation. Science *324*, 1076-1080.

West, A.P., Khoury-Hanold, W., Staron, M., Tal, M.C., Pineda, C.M., Lang, S.M., Bestwick, M., Duguay, B.A., Raimundo, N., MacDuff, D.A.*, et al.* (2015). Mitochondrial DNA stress primes the antiviral innate immune response. Nature *520*, 553-557.

Wiedemann, N., and Pfanner, N. (2017). Mitochondrial Machineries for Protein Import and Assembly. Annu Rev Biochem *86*, 685-714.

Wos, M., Szczepanowska, J., Pikula, S., Tylki-Szymanska, A., Zablocki, K., and Bandorowicz-Pikula, J. (2016). Mitochondrial dysfunction in fibroblasts derived from patients with Niemann-Pick type C disease. Arch Biochem Biophys.

Wu, Z., Puigserver, P., Andersson, U., Zhang, C., Adelmant, G., Mootha, V., Troy, A., Cinti, S., Lowell, B., Scarpulla, R.C.*, et al.* (1999). Mechanisms controlling mitochondrial biogenesis and respiration through the thermogenic coactivator PGC-1. Cell *98*, 115-124.

Yu, W., Gong, J.S., Ko, M., Garver, W.S., Yanagisawa, K., and Michikawa, M. (2005). Altered cholesterol metabolism in Niemann-Pick type C1 mouse brains affects mitochondrial function. J Biol Chem *280*, 11731-11739.

SUPPLEMENTARY MATERIALS

Supplementary Table I. Results of the promoter analysis of lysosomal genes. The transcription factor families that passed the significance threshold (Fisher exact test p<0.01) and the respective p-values are indicated.

Supplementary Table II. List of the transcription factors predicted to be significantly activated in the liver and brain of NPC1-/- mice compared to WT. The transcription factors and respective p-value is indicated. Transcription factors labelled in red were found to be significantly involved in both liver and brain of NPC1-/-, and thus selected for further analysis.

Supplementary Table III. List of primers. All primers used for quantitative real time PCR in this study are included in this table.

Supplementary Table IV. List of siRNA vectors. siRNAs for KLF2, ETV1 and a scrambled non-targeting control are included in this table with their corresponding sequences.